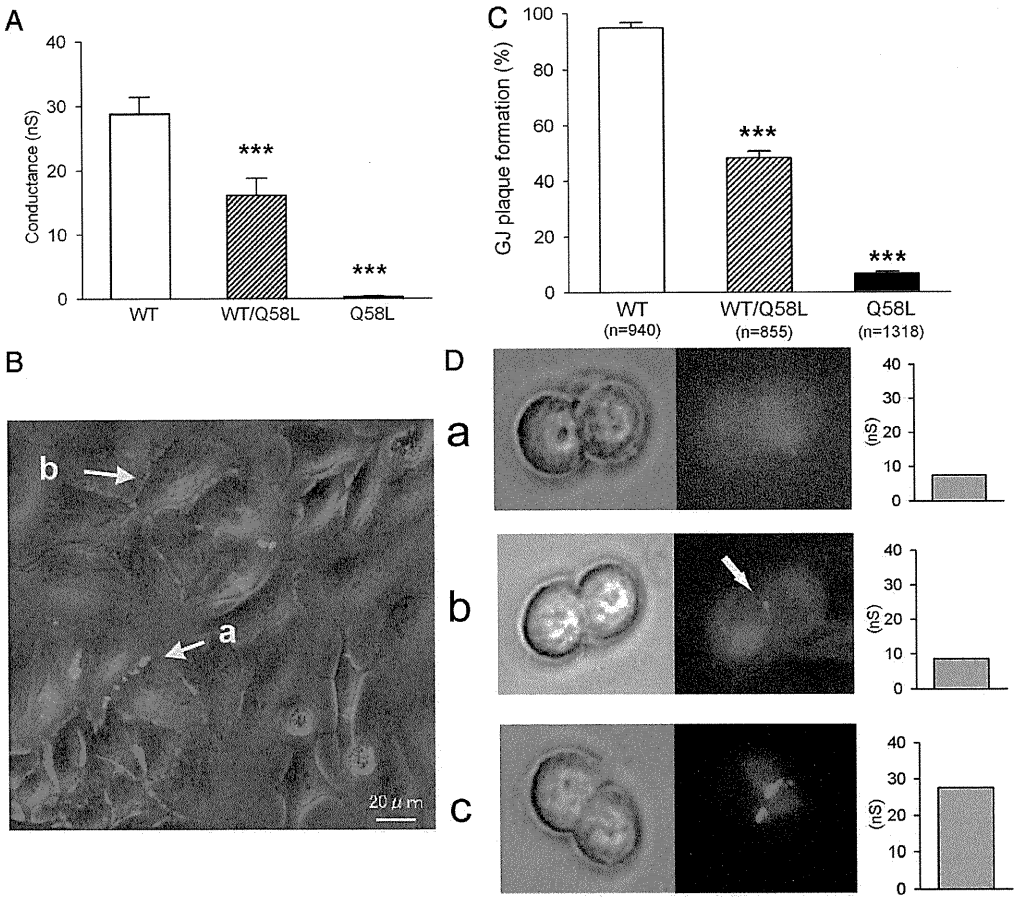

Figure 4. Macroscopic conductance and gap junction plaque morphology in cells coexpressing connexin40 (Cx40)-WT and Cx40-Q58L. **A**, Junctional conductance of cells transfected with plasmid pEGFPN1-Cx40-WT (1 μg), pEGFPN1-Cx40-Q58L (1 μg), or cotransfected with WT and Q58L (WT/Q58L, pEGFPN1-Cx40-WT 0.5μg+pEGFPN1-Cx40-Q58L 0.5 μg). **B**, Phase contrast/fluorescence overlay image of neuroblastoma cells transfected with WT/Q58L constructs. Arrow *a* points to gap junction plaque; arrow *b* points to an example of cells transfected but devoid of gap junction plaque. **C**, Efficacy of gap junction plaque formation was measured as the ratio between the number of gap junction plaque-positive cells and the number of fluorescent-positive cells (WT, n=940; WT/Q58L, n=855; Q58L, n=1318). **D**, Representative images of phase contrast (left), EGFP fluorescence (middle), and junctional conductance (right) from neuroblastoma cells cotransfected with pEGFPN1-Cx40-WT (0.25 μg) and pEGFPN1-Cx40-Q58L (0.25 μg). Three different examples illustrate the relation between plaque morphology and recorded junctional conductance. WT indicates wild type. ***$P<0.001$ compared with WT.

to the number of fluorescence-positive cells. In the Cx40-WT group, almost all fluorescent-positive cells exhibited clear gap junction plaques (94.9±1.9%, n=940), whereas there was a more-diffuse and homogenous pattern with only occasional plaque formation in the Cx40-Q58L group (6.6±0.7%, n=1318, $P<0.001$ compared with WT). In contrast, results varied widely in cells cotransfected with WT/Q58L; nearly one half of fluorescence-positive cells exhibited gap junction plaques similar to those observed in cells transfected with the WT construct (48.2±2.4%, n=855, $P<0.001$), whereas the rest showed a diffuse expression pattern similar to that of Cx40-Q58L. To establish a better correlation between plaque formation and junctional conductance, both variables were measured concurrently in the same cell pair for 39 N2A cell pairs where GFP-tagged plasmids of Cx40-WT and Cx40-Q58L were cotransfected. As shown in Figure 4D, about one half of GFP-positive cell pairs showed a very small Gj (<5 nS) and very few or negligible gap junction plaques (a). In the other half of cell pairs, small, dot-like junctional plaques correlated with intermediate Gj values (b), and there were clear, extensive gap junction plaques associated with Gj values >25 nS (c). Overall, we found significant heterogeneity in the extent of electric coupling, although the measurements of Gj correlated with the localization of proteins in transfected cells. These results indicate that the Q58L mutation significantly impairs the ability of cells to form gap junction plaques, although the effect is not purely dominant when both WT and mutant proteins are coexpressed.

Subcellular Distribution of WT and Q58L Cx40 in Transiently Transfected Cells

To further analyze the subcellular distribution of Cx40-WT and Cx40-Q58L proteins, the C terminal of Cx40-WT was

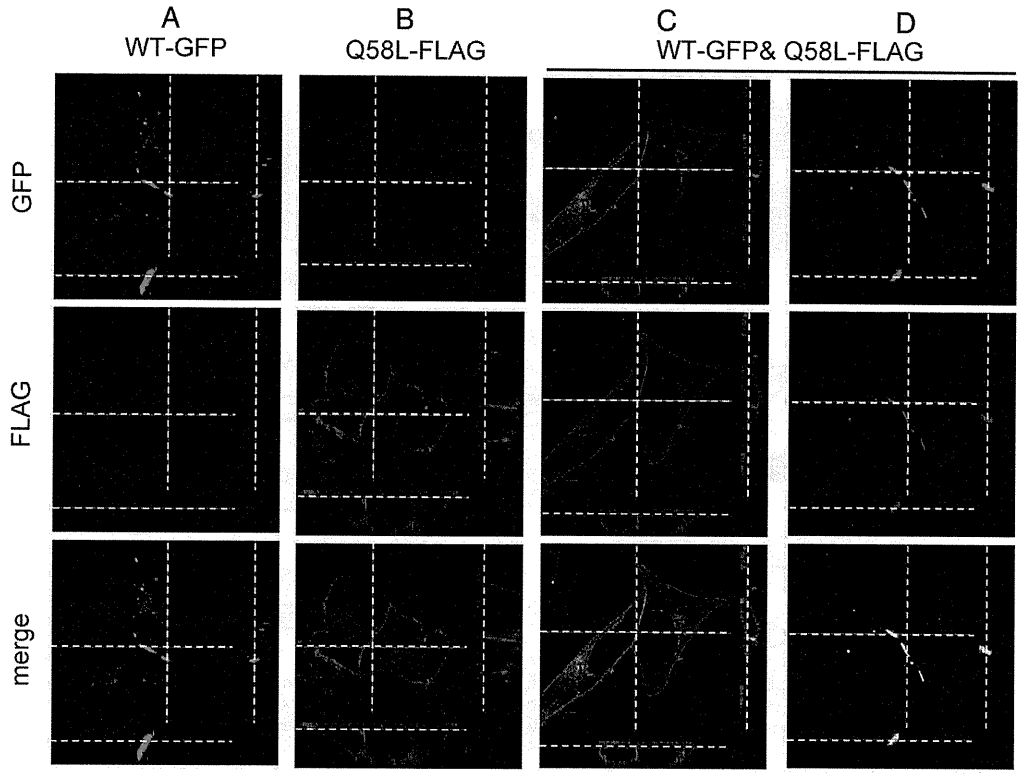

Figure 5. Subcellular distribution of connexin40 (Cx40)-WT and Cx40-Q58L in transiently transfected cells. HeLa cells were transiently transfected with pEGFPN1-Cx40-WT (3.0 μg) (**A**), pCMV-FLAG-Cx40-Q58L (3.0 μg) (**B**), or pEGFPN1-Cx40-WT (1.5 μg) plus pCMV-FLAG-Cx40-Q58L (1.5 μg) (**C**); immunostained for the respective tag protein; and visualized by confocal laser scanning microscopy. Notice that gap junction plaques (**A**) are absent in Q58L transfectants (**B**) and present in some (**D**) but not all (**C**) cotransfected cells. Bar=20 μm. WT indicates wild type.

tagged with GFP, whereas the C terminal of Cx40-Q58L was FLAG tagged. After transfection of N2A cells with the tagged constructs, the distribution of each protein was examined by confocal microscopy. As shown in Figure 5, green color indicates the position of GFP-tagged molecules, whereas red indicates the position of FLAG-tagged molecules. In cells transfected only with GFP-tagged Cx40-WT, fluorescence was consistently detected at sites of cell-cell apposition, following the pattern previously described for GFP-labeled gap junction plaques (Figure 5A). A similar distribution was found when cells were transfected with FLAG-tagged Cx40-WT (not shown). In contrast, most FLAG-tagged Cx40-Q58L signals were evenly distributed around the cell in the vicinity of the plasma membrane (Figure 5B). Biotinylation experiments showed that the Q58L mutation did not prevent the Cx40 protein from inserting into the membrane and presenting a domain-reachable form in the extracellular space (online-only Data Supplement Figure II). Micoscopy experiments in cells coexpressing GFP-tagged Cx40-WT and FLAG-tagged Cx40-Q58L proteins yielded results intermediate to those obtained when only 1 construct was expressed. Nearly one half of cell pairs showed that both proteins distributed homogenously at or near the cell membrane, without the formation of well-defined gap junction plaques (Figure 5C). These images resembled those obtained when only Cx40-Q58L proteins were expressed (Figure 5B, FLAG). In contrast, other cell pairs showed clustering of fluorescent signals within closely confined areas that appeared to be gap junction plaques (Figure 5D).

The experiments described herein led us to speculate that the distribution and function of heteromeric connexons is determined by their mutant subunit content, whereby formation (or not) of plaques and channels are determined, at least in part, by the abundance of expression of one protein over the other. As an initial step to probe this hypothesis, we took advantage of the characteristics of the bicistronic plasmid pIRES, in which the expression rate of the upstream gene is several-fold greater than that of the downstream gene,[20] and explored the functional properties of heteromeric connexons. Cx40-WT and GFP-tagged Cx40-Q58L were subcloned into the pIRES vector, either alone or in combination, in the specific orientations shown in Figure 6A. Protein expression levels of Cx40-WT and Cx40-Q58L were determined by immunochemistry. In contrast to the data obtained when Cx40-WT and GFP-tagged Cx40-Q58L plasmids were cotransfected at a 1:1 ratio (lane 6), expression of heteromeric pIRES plasmids WT-IRES-Q58L-EGFP (lane 3) and Q58L-EGFP-IRES-WT (lane 4) resulted in uneven protein expression levels of WT (40 kDa) and Q58L-EGFP (67 kDa), depending on their orientation in the pIRES vector. Based on

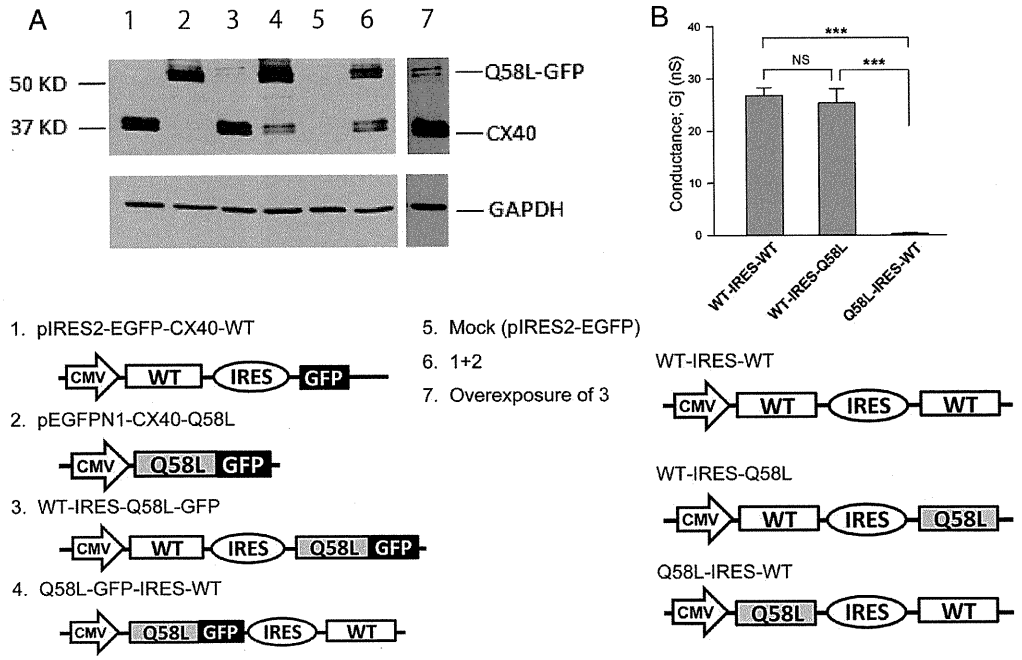

Figure 6. Mutant subunit abundance correlated with gap junction function. **A**, Neuroblastoma cells were transiently transfected with 3 μg Cx40 constructs in IRES plasmids. Cell lysates were analyzed by western blot using anti-Cx40 (top) and anti-GAPDH antibodies (bottom). The number in each lane corresponds to the plasmid noted below the image. Samples from cells cotransfected with plasmids 1 and 2 (1.5 μg each) were loaded on lane 6. Double bands of Cx40-WT (40 kDa) and Q58L-EGFP (67 kDa) are shown in lanes 3, 4, 6, and 7. Results were repeated in 3 separate experiments. Overexposure (lane 7) confirmed expression of the high-molecular-weight protein in lane 3. **B**, Junctional conductance of homomeric and heteromeric constructs (WT-IRES-Q58L and Q58L-IRES-WT). Conductance of cell pairs expressing WT-IRES-WT (n=17) was comparable to heteromeric construct WT-IRES-Q58L (n=17). However, converse heteromeric construct Q58L-IRES-WT (n=15) showed significantly reduced conductance ($P<0.001$ versus WT-IRES-WT and WT-IRES-Q58L). ***$P<0.001$. NS indicates not significant; WT, wild type.

these observations, we constructed a homomeric Cx40-WT plasmid (WT-IRES-WT) and heteromeric plasmids of Cx40-WT and Cx40-Q58L with different orientations (WT-IRES-Q58L and Q58L-IRES-WT) (Figure 6B). The junctional conductance of cell pairs expressing WT-IRES-Q58L (25.3±2.8 nS, n=17) was nearly indistinguishable from that of the homomeric plasmid WT-IRES-WT (27.8±1.4 nS, n=17, *P* not significant). By contrast, the converse heteromeric construct Q58L-IRES-WT showed substantially reduced junctional conductance (0.29±0.12 nS, n=15, $P<0.001$) comparable with that of the homomeric Q58L (0.56±0.34 nS) (Figure 3A). These results suggest that the final electrophysiological properties of the heteromeric connexons are determined predominantly by the numbers of mutant subunits in each gap junction rather than defined by a dominant-negative effect.

Discussion

Genetic screening confirmed the association of *SCN5A* and *SCN1B* with PFHB1[13–15] and revealed novel mutations within these genes (online-only Data Supplement Table I). More importantly, we identified a particularly severe, early onset case of PFHBI associated with a germ line mutation in *GJA5* in 2 blood relatives (proband and sister) given a clinical diagnosis of PFHBI. The data also indicate that the protein expressed (Cx40-Q58L) failed to form functional gap junctions in an exogenous expression system and decreased the probability of gap junction formation in cells coexpressing the WT protein.

So far, *SCN5A*, *SCB1B*, and *TRPM4* are the only genes associated with PFHB1.[11,13,14] The National Human Genome Research Institute database shows no association of *GJA5* single-nucleotide polymorphisms with arrhythmias or conduction system diseases. PR interval and QRS have been associated with several loci, including *SCN5A*, *SCN10A*, *NKX2.5*, and *TBX5*[21,22] but not *GJA5*, which is located at chromosome 1q21.1. Overall, the present results suggest that *GJA5* is a candidate gene associated with PFHBI, likely in a small fraction of the affected population. Yet, given the limited cosegregation observed in the reported family, we remain cautious in assigning a causative nature to the *GJA5* mutation. It will be of great interest to expand the screening of *GJA5* at the research level to identify other cases associated with amino acid changes in Cx40, although it may be premature to include *GJA5* as a part of the routine diagnostic screen.[17] The present results also emphasize the importance of Cx40 in the maintenance of normal cardiac rhythm.

To our knowledge, this is the first report of a germ line mutation in Cx40 associated with a high risk of ventricular arrhythmias (online-only Data Supplement Figure II). Other studies have shown somatic mutations of Cx40 or Cx43 in patients with idiopathic atrial fibrillation[5,23]; those mutations

were confined to the atria, and conduction abnormalities in the ventricles or His-Purkinje system were not observed. On the other hand, as in all cases involving identified genetic substrates for disease, the possibility of compound mutations in unexamined genes cannot be excluded. We do emphasize that the mutation led to a severe cellular phenotype in an exogenous expression system, supporting the argument that just the Q58L substitution can impair the formation of gap junctions necessary for propagation of action potentials between cells.

The results show that Cx40-Q58L was abundantly expressed in an exogenous system. The protein reached the vicinity of the cell membrane but failed to form gap junction plaques (Figure 5B). This result may be due to impaired docking of mutant hemichannels within the intercellular space because of the mutation in the extracellular loop (Figure 1C). During trafficking, connexin subunits oligomerize to form a hemichannel (or connexon). Once at the site of cell contact, connexons from apposing cells dock, sealing the hydrophilic path (the channel pore) from the extracellular space. The locking of 2 connexons into 1 gap junction channel is believed to stabilize connexin subunits in place, facilitating aggregation of other oligomers into their vicinity and eventually forming a plaque. Amino acid substitutions within the extracellular loop, as in Q58L, can prevent hemichannel docking and, thus, plaque formation.[24] The present biotinylation experiments indicate that the Q58L protein integrates into the cell membrane, supporting the notion that the inability of the Q58L mutation to form functional gap junctions is related to events that occur after the oligomer is delivered to the cell membrane and before a functional dodecamer converts into a functional channel in a gap junction plaque.

Results obtained in cells coexpressing both mutant and WT proteins clearly show that one subunit can significantly influence the fate of the other (Figure 5). This suggests that Cx40-Q58L subunits retain their ability to oligomerize not only with other mutant subunits, but also with the WT protein. The results also present an interesting paradigm in that neither the WT nor the mutant construct exerted a dominant effect over the other. After transfection with equal amounts of cDNA, we found cells where both WT and mutant proteins displayed the phenotype of the mutant construct, whereas in other cases, junctional plaques could be easily discerned (although an outline of the cell, likely resulting from the presence of the FLAG-tagged mutant protein, could still be observed [see red signal in Figure 5D]). These results can be explained if we assume that the probability of proper targeting and integration of a connexon into a plaque decreases as a function of the number of mutant subunits contained. For cotransfection, we used equal amounts of cDNA; however, it is very likely that each cell was transfected with variable amounts of each construct and, thus, expressed variable amounts of each protein. We speculate that a majority (though of unknown stoichiometry) of WT connexin subunits are required in a connexon for proper formation of functional gap junctions. Thus, if a cell captures an abundance of Q58L cDNA, most oligomers will contain an excess of mutant subunits, and gap junction formation will fail. If, on the other hand, that cell captures and expresses more of the WT cDNA, the distribution of the subunits within the oligomer will contain a majority of WT connexins, and the connexon will be properly integrated into a channel. This hypothesis will require further testing, although data presented in Figure 6 support the concept that success or failure of functional channel formation may relate to relative abundance of each protein (WT or mutant). If our hypothesis is correct, it suggests that the distribution of functional gap junctions in the His-Purkinje network of affected individuals could vary significantly among cells, depending on the extent of expression of each allele in each cell. The resulting phenotype may be that of a Purkinje network where gap junction-mediated coupling could be heterogeneous, setting the stage for local conduction block, microreentry, and ventricular arrhythmias at the Purkinje network or at the Purkinje-muscle junction.[1,2]

Overall, we show that both proband and sister have a genotype that (1) is absent in hundreds of control subjects and in the unaffected parent (the father), (2) disrupts an important functional domain of the protein, and (3) disrupts the formation of gap junction channels. The data therefore support the notion of an association between the Cx40 mutation and the clinical phenotype and emphasize the importance of future studies to assess the possible involvement of Cx40 mutations as causative of the disease.

Acknowledgments

We thank Dr A.L. George for critical reading of the manuscript and Mss M. Fukuoka and C.R. Ingram for technical assistance.

Sources of Funding

This work was supported by research grant 21590921 (to Dr Makita), Scientific Research B (to Dr Mochizuki), and Grant-in-Aid for Scientific Research on Innovative Areas (HD Physiology) 22136007 (to Dr Makita) from the Ministry of Education, Culture, Sports, Science and Technology, Japan; a Health and Labor Sciences Research Grant for research on measures for intractable diseases from the Ministry of Health (2010-145) (to Dr Makita); the Mitsubishi Pharma Research Foundation (to Dr Makita); the Japan-France Integrated Action Program (SAKURA) (to Drs Makita and Schott); The Naito Foundation (to Drs Makita and Seki); the Support Center for Women Health Care Professionals and Researchers 21590921 (to Dr Seki); and grants GM057691, HL106632 and HL087226 from the National Institutes of Health (to Dr Delmar).

Disclosures

None.

References

1. Saffitz JE, Lerner DL, Yamada KA. Gap junction distribution and regulation in the heart. In: Zipes DP, Jalife J, eds. *Cardiac Electrophysiology: From Cell to Bedside.* Philadelphia, PA: Saunders; 2004:181–191.
2. Park DS, Fishman GI. The cardiac conduction system. *Circulation.* 2011; 123:904–915.
3. Ruan Y, Liu N, Priori SG. Sodium channel mutations and arrhythmias. *Nat Rev Cardiol.* 2009;6:337–348.
4. Firouzi M, Ramanna H, Kok B, Jongsma HJ, Koeleman BPC, Doevendans PA, Groenewegen WA, Hauer RNW. Association of human connexin40 gene polymorphisms with atrial vulnerability as a risk factor for idiopathic atrial fibrillation. *Circ Res.* 2004;95:e29–e33.
5. Gollob MH, Jones DL, Krahn AD, Danis L, Gong X-Q, Shao Q, Liu X, Veinot JP, Tang ASL, Stewart AFR, Tesson F, Klein GJ, Yee R, Skanes AC, Guiraudon GM, Ebihara L, Bai D. Somatic mutations in the connexin 40 gene (*GJA5*) in atrial fibrillation. *N Engl J Med.* 2006;354:2677–2688.

6. Lenègre J. Etiology and pathology of bilateral bundle branch block in relation to complete heart block. *Prog Cardiovasc Dis.* 1964;6:409–444.
7. Lev M, Kinare SG, Pick A. The pathogenesis of atrioventricular block in coronary disease. *Circulation.* 1970;42:409–425.
8. Probst V, Kyndt F, Potet F, Trochu JN, Mialet G, Demolombe S, Schott JJ, Baro I, Escande D, Le Marec H. Haploinsufficiency in combination with aging causes SCN5A-linked hereditary Lenègre disease. *J Am Coll Cardiol.* 2003;41:643–652.
9. Brink PA, Ferreira A, Moolman JC, Weymar HW, van der Merwe P-L, Corfield VA. Gene for progressive familial heart block type I maps to chromosome 19q13. *Circulation.* 1995;91:1633–1640.
10. de Meeus A, Stephan E, Debrus S, Jean M-K, Loiselet J, Weissenbach J, Demaille J, Bouvagnet P. An isolated cardiac conduction disease maps to chromosome 19q. *Circ Res.* 1995;77:735–740.
11. Kruse M, Schulze-Bahr E, Corfield V, Beckmann A, Stallmeyer B, Kurtbay G, Ohmert I, Schulze-Bahr E, Brink P, Pongs O. Impaired endocytosis of the ion channel TRPM4 is associated with human progressive familial heart block type I. *J Clin Invest.* 2009;119:2737–2744.
12. Royer A, van Veen TAB, Le Bouter S, Marionneau C, Griol-Charhbili V, Leoni A-L, Steenman M, van Rijen HVM, Demolombe S, Goddard CA, Richer C, Escoubet B, Jarry-Guichard T, Colledge WH, Gros D, de Bakker JMT, Grace AA, Escande D, Charpentier F. Mouse model of SCN5A-linked hereditary Lenègre's disease. Age-related conduction slowing and myocardial fibrosis. *Circulation.* 2005;111:1738–1746.
13. Schott JJ, Alshinawi C, Kyndt F, Probst V, Hoorntje TM, Hulsbeek M, Wilde AA, Escande D, Mannens MM, Le Marec H. Cardiac conduction defects associate with mutations in SCN5A. *Nat Genet.* 1999;23:20–21.
14. Watanabe H, Koopmann TT, Le Scouarnec S, Yang T, Ingram CR, Schott JJ, Demolombe S, Probst V, Anselme F, Escande D, Wiesfeld AC, Pfeufer A, Kaab S, Wichmann HE, Hasdemir C, Aizawa Y, Wilde AA, Roden DM, Bezzina CR. Sodium channel beta1 subunit mutations associated with Brugada syndrome and cardiac conduction disease in humans. *J Clin Invest.* 2008;118:2260–2268.
15. McNair WP, Ku L, Taylor MRG, Fain PR, Dao D, Wolfel E, Mestroni L; Familial Cardiomyopathy Registry Research Group. SCN5A mutation associated with dilated cardiomyopathy, conduction disorder, and arrhythmia. *Circulation.* 2004;110:2163–2167.
16. Miquerol L, Meysen S, Mangoni M, Bois P, van Rijen HVM, Abran P, Jongsma H, Nargeot J, Gros D. Architectural and functional asymmetry of the His-Purkinje system of the murine heart. *Cardiovasc Res.* 2004; 63:77–86.
17. Ackerman MJ, Priori SG, Willems S, Berul C, Brugada R, Calkins H, Camm AJ, Ellinor PT, Gollob M, Hamilton R, Hershberger RE, Judge DP, Le Marec H, McKenna WJ, Schulze-Bahr E, Semsarian C, Towbin JA, Watkins H, Wilde A, Wolpert C, Zipes DP. HRS/EHRA expert consensus statement on the state of genetic testing for the channelopathies and cardiomyopathies. *Heart Rhythm.* 2011;8:1308–1339.
18. Seki A, Coombs W, Taffet SM, Delmar M. Loss of electrical communication, but not plaque formation, after mutations in the cytoplasmic loop of connexin43. *Heart Rhythm.* 2004;1:227–233.
19. Anumonwo JMB, Taffet SM, Gu H, Chanson M, Moreno AP, Delmar M. The carboxyl terminal domain regulates the unitary conductance and voltage dependence of connexin40 gap junction channels. *Circ Res.* 2001;88:666–673.
20. Bochkov YA, Palmenberg AC. Translational efficiency of EMCV IRES in bicistronic vectors is dependent upon IRES sequence and gene location. *Biotechniques.* 2006;41:283–284.
21. Holm H, Gudbjartsson DF, Arnar DO, Thorleifsson G, Thorgeirsson G, Stefansdottir H, Gudjonsson SA, Jonasdottir A, Mathiesen EB, Njolstad I, Nyrnes A, Wilsgaard T, Hald EM, Hveem K, Stoltenberg C, Lochen M-L, Kong A, Thorsteinsdottir U, Stefansson K. Several common variants modulate heart rate, PR interval and QRS duration. *Nat Genet.* 2010;42:117–122.
22. Pfeufer A, van Noord C, Marciante KD, Arking DE, Larson MG, Smith AV, Tarasov KV, Muller M, Sotoodehnia N, Sinner MF, Verwoert GC, Li M, Kao WHL, Kottgen A, Coresh J, Bis JC, Psaty BM, Rice K, Rotter JI, Rivadeneira F, Hofman A, Kors JA, Stricker BHC, Uitterlinden AG, van Duijn CM, Beckmann BM, Sauter W, Gieger C, Lubitz SA, Newton-Cheh C, Wang TJ, Magnani JW, Schnabel RB, Chung MK, Barnard J, Smith JD, Van Wagoner DR, Vasan RS, Aspelund T, Eiriksdottir G, Harris TB, Launer LJ, Najjar SS, Lakatta E, Schlessinger D, Uda M, Abecasis GR, Muller-Myhsok B, Ehret GB, Boerwinkle E, Chakravarti A, Soliman EZ, Lunetta KL, Perz S, Wichmann HE, Meitinger T, Levy D, Gudnason V, Ellinor PT, Sanna S, Kaab S, Witteman JCM, Alonso A, Benjamin EJ, Heckbert SR. Genome-wide association study of PR interval. *Nat Genet.* 2010;42:153–159.
23. Thibodeau IL, Xu J, Li Q, Liu G, Lam K, Veinot JP, Birnie DH, Jones DL, Krahn AD, Lemery R, Nicholson BJ, Gollob MH. Paradigm of genetic mosaicism and lone atrial fibrillation: physiological characterization of a connexin 43-deletion mutant identified from atrial tissue. *Circulation.* 2010;122:236–244.
24. Sosinsky GE, Nicholson BJ. Structural organization of gap junction channels. *Biochim Biophys Acta.* 2005;1711:99–125.

CLINICAL PERSPECTIVE

Progressive familial heart block type I, also known as progressive cardiac conduction defect, is an inherited form of cardiac conduction system dysfunction that can lead to severe heart rhythm disturbances, including sudden cardiac death. The genetic causes of this disease are poorly understood. Here, we genetically screened 156 patients with progressive familial heart block type I. In addition to mutations in genes of the voltage-gated cardiac sodium channel complex (*SCN5A* and *SCN1B*), we found a novel germ line mutation in *GJA5*, the gene encoding the gap junction protein connexin40. The disease had an early onset and was associated with otherwise unexplained sudden cardiac death in the proband and his mother. The proband's sister is also affected. Cellular phenotype analysis revealed impaired gap junction formation at cell-cell interfaces and marked reduction of junctional conductance in cells expressing the mutated connexin40 protein. The results emphasize the importance of connexin40 in normal electrical propagation in the cardiac conduction system and open the possibility of including *GJA5* as a target gene for study in patients with progressive familial heart block type I.

Regional cooling facilitates termination of spiral-wave reentry through unpinning of rotors in rabbit hearts

Masatoshi Yamazaki, MD, PhD,*† Haruo Honjo, MD, PhD,* Takashi Ashihara, MD, PhD,‡ Masahide Harada, MD, PhD,* Ichiro Sakuma, PhD,§ Kazuo Nakazawa, PhD,‖ Natalia Trayanova, PhD, FHRS, FAHA,¶ Minoru Horie, MD, PhD,‡ Jérôme Kalifa, MD, PhD,† José Jalife, MD, FHRS,† Kaichiro Kamiya, MD, PhD,* Itsuo Kodama, MD, PhD*

*From the *Department of Cardiovascular Research, Research Institute of Environmental Medicine, Nagoya University, Nagoya, Japan, †Center for Arrhythmia Research, University of Michigan, Ann Arbor, Michigan, ‡Department of Cardiovascular and Respiratory Medicine, Shiga University of Medical Science, Otsu, Japan, §Graduate School of Engineering, The University of Tokyo, Tokyo, Japan, ‖National Cardiovascular Center, Research Institute, Suita, Japan, ¶Institute for Computational Medicine, Johns Hopkins University, Baltimore, Maryland.*

BACKGROUND Moderate global cooling of myocardial tissue was shown to destabilize 2-dimensional (2-D) reentry and facilitate its termination.

OBJECTIVE This study sought to test the hypothesis that regional cooling destabilizes rotors and facilitates termination of spontaneous and DC shock-induced subepicardial reentry in isolated, endocardially ablated rabbit hearts.

METHODS Fluorescent action potential signals were recorded from 2-D subepicardial ventricular myocardium of Langendorff-perfused rabbit hearts. Regional cooling (by 5.9°C ± 1.3°C) was applied to the left ventricular anterior wall using a transparent cooling device (10 mm in diameter).

RESULTS Regional cooling during constant stimulation (2.5 Hz) prolonged the action potential duration (by 36% ± 9%) and slightly reduced conduction velocity (by 4% ± 4%) in the cooled region. Ventricular tachycardias (VTs) induced during regional cooling terminated earlier than those without cooling (control): VTs lasting >30 seconds were reduced from 17 of 39 to 1 of 61. When regional cooling was applied during sustained VTs (>120 seconds), 16 of 33 (48%) sustained VTs self-terminated in 12.5 ± 5.1 seconds. VT termination was the result of rotor destabilization, which was characterized by unpinning, drift toward the periphery of the cooled region, and subsequent collision with boundaries. The DC shock intensity required for cardioversion of the sustained VTs decreased significantly by regional cooling (22.8 ± 4.1 V, n = 16, vs 40.5 ± 17.6 V, n = 21). The major mode of reentry termination by DC shocks was phase resetting in the absence of cooling, whereas it was unpinning in the presence of cooling.

CONCLUSION Regional cooling facilitates termination of 2-D reentry through unpinning of rotors.

KEYWORDS Spiral-wave reentry; Regional myocardial cooling; Unpinning; Optical mapping; Ventricular tachyarrhythmia

ABBREVIATIONS **2-D** = two-dimension; **3-D** = three-dimension; **APD** = action potential duration; **BCL** = basic cycle length; **BDM** = 2,3-butandione monoxime; **CV** = conduction velocity; **FBL** = functional block line; **ICD** = implantable cardioverter-defibrillator; **LV** = left ventricle; **PS** = phase singularity; **RC** = regional cooling; **SW** = spiral wave; **VF** = ventricular fibrillation; **VT** = ventricular tachycardia

(Heart Rhythm 2012;9:107–114)

Introduction

High-energy DC shock application by implantable cardioverter-defibrillator (ICD) is the most effective procedure for preventing sudden cardiac death resulting from ventricular tachycardia/ventricular fibrillation (VT/VF). Large-scale clinical trials have demonstrated that ICD therapy is superior over any pharmacological therapy to prevent cardiac death.[1,2] The usefulness of ICD therapy currently available is, however, limited by a number of adverse effects of high-energy shocks, such as myocardial damages causing arrhythmias, increased pacing threshold,[3,4] and mechanical dysfunction giving rise to hemodynamic deterioration.[5] In addition, painful DC shocks by ICD often cause serious psychological disorders.[6,7] Theoretical and experimental studies have revealed that spiral-wave (SW) reentry rotating around a functional obstacle is the major mechanism of VT/VF.[8,9] Arguably, should SW reentry be regulatable by procedures other than DC shocks or those combined with low-energy shocks, it could lead to innovative therapeutic

This study was supported by Grant-in-Aid for Scientific Research (B) 19390210 and (C) 20590860 from the Japanese Society for Promotion of Sciences and Grant-in-Aid for Scientific Research on Innovative Area 22136010 from the Ministry of Education, Culture, Sports, Science and Technology, Japan. **Address reprint requests and correspondence:** Dr. Haruo Honjo, Department of Cardiovascular Research, Research Institute of Environmental Medicine, Nagoya University, Furo-cho, Chikusa-ku, Nagoya 464-8601, Japan. E-mail address: honjo@riem.nagoya-u.ac.jp.

1547-5271/$ -see front matter doi:10.1016/j.hrthm.2011.08.013

modalities for prevention of arrhythmic death. Although several conceptual approaches have been proposed to terminate SW reentry by low-energy DC application, e.g., resonant drift,[10,11] controlling chaos,[12] synchronized pacing,[13,14] and unpinning of SWs,[15,16] feasibility of these approaches has not yet been validated. In isolated rabbit hearts, we have previously shown that moderate hypothermia facilitates termination of VT through destabilization (unpinning) of SW reentry.[17] Using high-density electrode mapping in rabbit hearts, Boersma et al[18] demonstrated that regional cooling (RC) of the ventricle during programmed electrical stimulation prevented stabilization of functional reentry and resulted in only brief episodes of polymorphic VT that terminated spontaneously. Here we hypothesized that moderate RC of the ventricular myocardium could be a novel procedure to destabilize already-established and sustained VT and lead to its termination. To test this hypothesis, we carried out high-resolution optical mapping experiments in 2-dimensional (2-D) ventricular myocardium.

Methods

Experimental model and optical mapping

The protocol was approved by the Institutional Animal Care and Use Committee at Nagoya University. The experimental model and procedures of optical mapping are essentially the same as reported previously.[17,19,20] Briefly, optical membrane potential signals were recorded from a 2-D ventricular muscle layer of Langendorff-perfused rabbit hearts subjected to endocardial cryoablation; 2,3-butandione monoxime (BDM) was applied to minimize motion artifacts. Action potential duration (APD) and conduction velocity (CV) were measured during constant pacing (basic cycle length [BCL] 180 to 400 ms) from the apex. The details of experimental procedures and data analysis are described in the Online Supplemental Methods.

RC

The temperature of the central region of the left ventricular (LV) free wall was temporarily reduced by applying a transparent cooling device (diameter, 10 mm) perfused with cold water and in abutting contact with the epicardial surface (Figure 1A). In pilot experiments using thermography (TVS-200, Nippon Avionics, Tokyo, Japan) (Figure 1B), we confirmed that the temperature in the target area was decreased by 5.9°C ± 1.3°C (n = 7, $P < .05$) from baseline (36.0°C). The temperature change was reversed completely after removal of the device. Temperature outside the cooled region remained unchanged.

Experimental protocols

Reentrant VTs (lasting ≥3 beats) were induced by modified cross-field stimulation using 1 of 2 protocols. First, in 8 hearts, VTs were induced before and 20 seconds after application of RC to compare their duration and dynamics. Second, in 15 additional hearts, sustained VTs (>120 seconds) were induced and RC was applied to observe its effects on VT duration and dynamics. If the sustained VTs did not terminate during the 30-second observation period of RC, 10-ms monophasic DC shocks were applied at in-

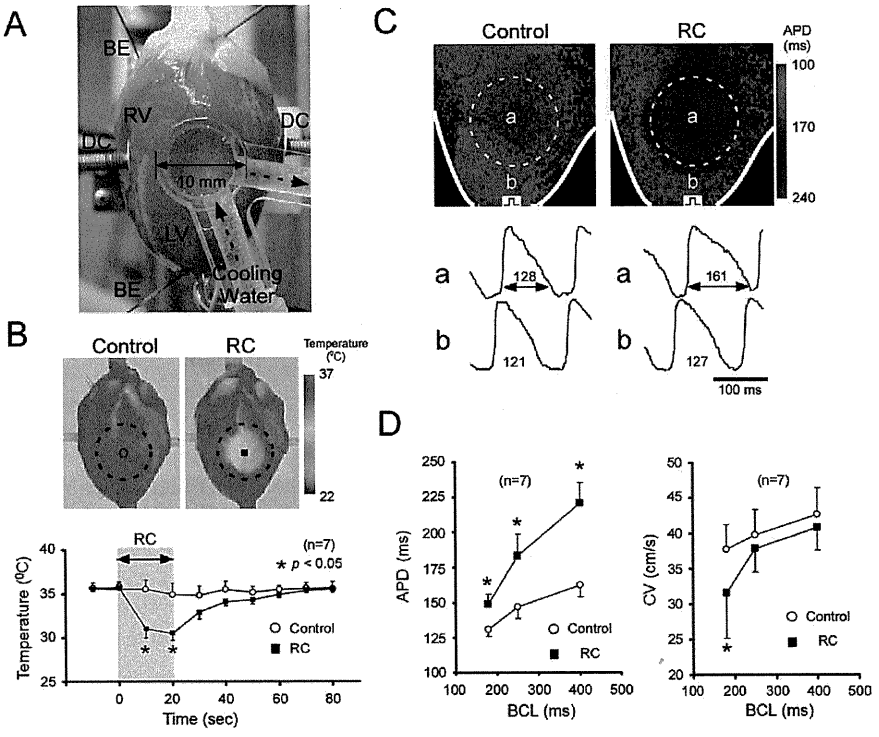

Figure 1 RC of 2-D rabbit hearts. **A:** A transparent cooling device (diameter, 10 mm) was in contact with the LV subepicardial surface, and water (20°C) was circulated inside the device. **B:** Thermography images (top) and changes of temperature (bottom) in response to RC. Those without RC served as control. *$P < .05$ vs control. **C:** Changes of APD (BCL, 400 ms) in response to RC. Top, APD color gradient maps with and without RC (control); bottom, optical action potential signals inside (a) and outside (b) the RC region. Numerals are APD (in ms). **D:** Effects of RC on APD (left) and CV (right) in the RC region at BCLs 180 to 400 ms. *$P < .05$ vs control (without RC). 2-D = two-dimension; APD = action potential duration; BCL = basic cycle length; BE = electrodes for recording distant bipolar electrograms; CV = conduction velocity; DC = paddle electrodes for DC-application; LV = left ventricle; RC = regional cooling.

creasing or decreasing voltage (by 5 to 10 V in steps from 25 V) to determine the threshold intensity for cardioversion. Sustained VTs without RC served as control subjects.

In 6 rabbits, effects of RC on VT/VF were examined in 3-dimensional (3-D) ventricles without cryoablation. Sustained VT/VFs (>120 seconds) were induced, and cardioversion by RC alone or in combination with DC shocks (8/2-ms biphasic, 25 to 100 V) was attempted.

Statistical analysis

Data are expressed as mean ± SD. Statistical comparisons were performed by 2-way analysis of variance with Bonferroni post hoc test or Welch 2-sample t test when appropriate. Differences were considered significant when $P < .05$.

Results

APD and CV during constant pacing

Effects of RC on APD and CV were examined in 7 hearts. Representative changes in APD (BCL, 400 ms) are shown in Figure 1C. Cooling (20 seconds) increased APD in the RC region, whereas APD outside the RC region was unchanged. Figure 1D summarizes the changes of APD and CV in the RC region. RC caused a significant increase of APD (BCLs, 180 to 400 ms); the longer the BCL, the greater the APD prolongation. RC decreased CV, although the changes remained statistically insignificant at BCLs 250 and 400 ms.

In 3 hearts, all of the RC-induced changes of APD and CV were reversed completely within 60 seconds after removal of the cooling device (data not shown).

VT induced during RC application

In 8 hearts, VTs were induced before (control) and 20 seconds after RC. In control subjects, 18 of 39 VTs (46%) terminated within 5 seconds, 4 VTs (10%) terminated in 5 to 30 seconds, and 17 VTs (44%) persisted for >30 seconds. During RC, in contrast, 58 of 61 VTs (95%) terminated within 5 seconds, 2 TVs (3%) terminated in 5 to 30 seconds, and 1 VT (2%) persisted >30 seconds. Thus, most of VTs induced during RC terminated earlier than in control subjects. The VT cycle length during RC (178 ± 20 ms, n = 61) was significantly longer compared with control subjects (143 ± 23 ms, n = 39, $P < .05$). Reversibility of the RC effects on the VT persistence was tested in 3 hearts. The incidence of persisted (>30 seconds)/all VTs was 11 of 23 (48%) in control subjects, 1 of 26 (4%) during RC, and 8 of 13 (62%) 5 to 20 minutes after removal of the cooling device.

Optical images of excitation were analyzed in 5 hearts (9 VTs before RC and 13 VTs during RC) exhibiting visible rotor(s). In control, the rotors were, in most cases (7 of 9) stable with small meandering. The 13 VTs induced during RC, in contrast, were all unstable with remarkable meandering of rotors along the periphery of the RC region, and they terminated shortly. Action potential traces revealed frequent intermittent conduction block in the RC region with longer APD, giving rise to drift of the reentry circuit (Online Supplementary Figure 1). The rotors terminated by collision with anatomical boundaries in 7 VTs (Online Supplementary Figure 1), whereas by mutual annihilation in the RC region in 2 cases (Online Supplementary Figure 2). The mode of rotor termination was unable to be analyzed in the remaining 4 cases.

Termination of sustained VT by RC

We next examined the effects of RC applied during sustained VTs (lasting >120 seconds). We induced 76 sustained VTs in 15 hearts and observed them for 30 seconds with and without RC (33 VTs with RC, and 43 VTs without RC as control subjects). None of the 43 sustained VTs terminated in control subjects, whereas 16 of 33 (48%) sustained VTs terminated during the observation period with RC. Average time to termination was 12.5 ± 5.1 seconds (n = 16).

Optical images of excitation were analyzed in 16 sustained VTs that terminated during the RC application in 8 hearts. Figure 2 shows a representative experiment. Before the RC application, a stable clockwise rotor circulated around a functional block line (FBL) (approximately 5.1 mm); the bipolar electrogram showed a monomorphic pattern (Figure 2A, and Online Supplementary Video 1). A 3-D plot of the phase singularity (PS) trajectory obtained after phase mapping confirmed the stationarity of the rotor activity. Application of RC resulted in a dramatic change of the rotor dynamics and the VT terminated after approximately 10 seconds. Figure 2B shows isochrone maps during the last 3 beats prior to VT termination. A clockwise rotor circulated around a very long and curved FBL in the RC region in beat 1 and 2. The FBL configuration changed beat to beat in such a way that during beat 3 the FBL extended from the RC region to the atrioventricular groove, resulting in termination of reentry. The bipolar electrogram showed a polymorphic pattern before termination. Action potentials (Figure 2C) from the RC region (d) were longer compared with those outside (a–c, e, f), and this provided a substrate for conduction block. In Figure 2D, phase maps (left) and a 3-D plot of the PS trajectory (right) demonstrated that a single PS moved along the periphery of the RC region and collided with the atrioventricular groove (Online Supplementary Video 2). The mode of rotor termination by RC could be analyzed in 6 sustained VTs. In 4 sustained VTs, rotor terminated by drift and subsequent collision of PSs with boundaries, whereas in the remaining 2 cases, by mutual annihilation of PSs with opposite chiralities in the RC region.

RC failed to terminate 17 of 33 (52%) of the sustained VTs. The failure was attributable in part to the topological relationship between the rotor and the RC region. In other words, the success rate of RC cardioversion was relatively high (12 of 19) when the rotation center was located within or in the vicinity of the RC region. However, success was low (4 of 14) when the rotation center was far from the RC region.

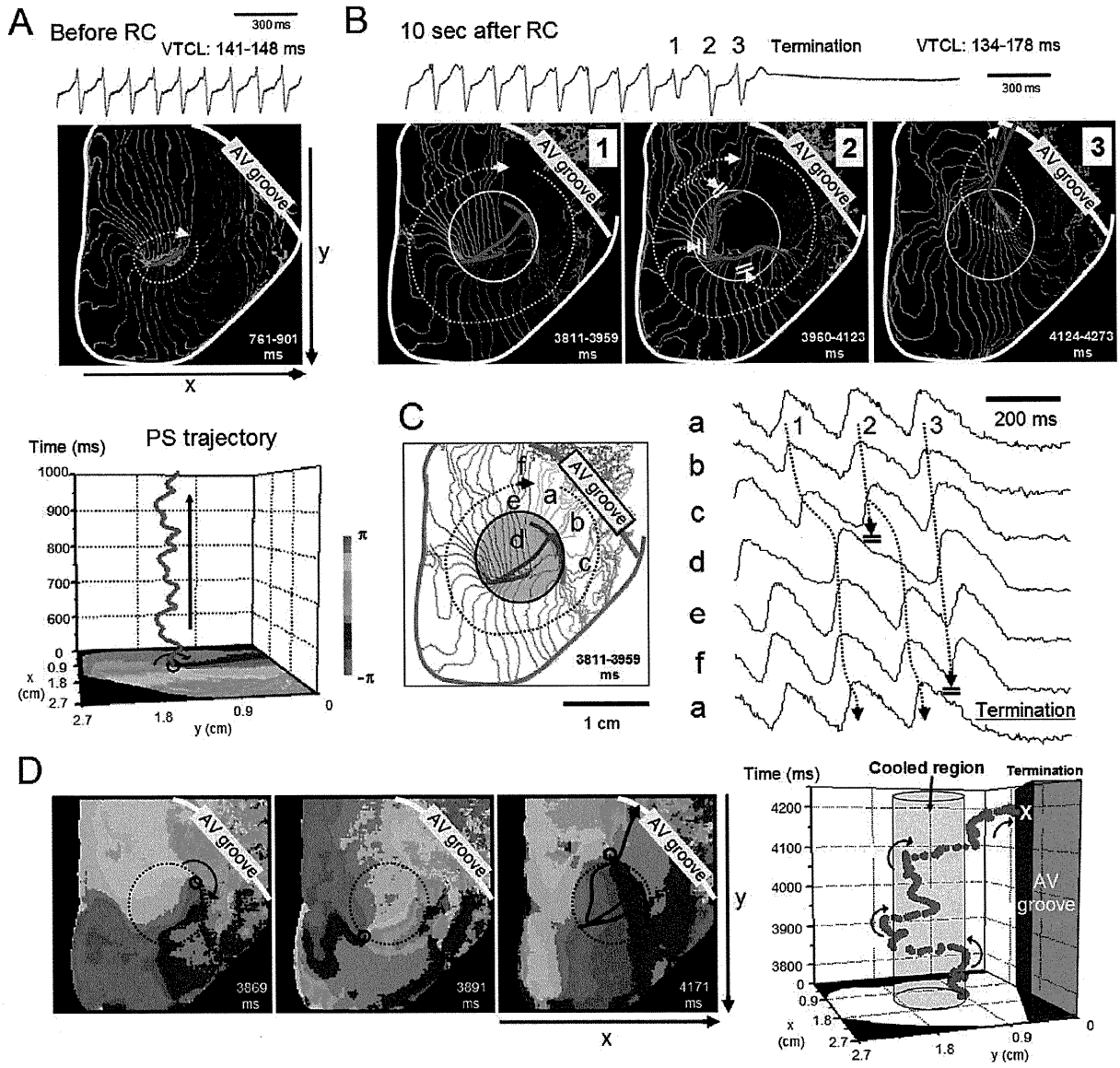

Figure 2 Termination of sustained VT by RC. **A:** Bipolar electrogram (top) and 4-ms isochrone map (middle) of sustained VT (>120 seconds) before RC application. Bottom, trajectory of a PS plotted on space-time axes. Stable reentrant activity was maintained. **B:** Bipolar electrogram (top) and isochrone maps (bottom) of 3 consecutive beats prior to VT termination approximately 10 seconds after RC. A clockwise rotor rotating around a long and curved FBL (pink) changed circuits in each excitation. Yellow circle, RC region. **C:** Optical action potential signals (a–f in the isochrone map) prior to VT termination. Wave propagation was frequently blocked at the periphery of the RC region. **D:** Left, phase maps of the last 2 beats. Black circle, PS of clockwise rotation; dotted circle, RC region. Right, PS trajectory plotted on space-time axes. Blue column, RC region. PS = phase singularity; VT = ventricular tachycardia; other abbreviations as in Figure 1.

Cardioversion of sustained VT by DC shock

When the sustained VTs did not terminate during the 30-second observation period, DC cardioversion was attempted. DC shocks of 15 to 80 V were applied to 21 sustained VTs in the absence of RC (in 12 hearts) and 16 sustained VTs in presence of RC (in 9 hearts) to evaluate the threshold DC shock intensity for cardioversion. The threshold DC shock intensity required for VT termination was significantly less with RC (22.8 ± 4.1 V, n = 16) than that without RC (40.5 ± 17.6 V, n = 21, $P < .05$).

The mode of rotor modification and termination by DC shocks with and without RC was also different. Representative experiments are shown in Figure 3. Figure 3A is the consequence of a 25-V shock that failed to terminate the reentrant activity in the absence of RC. A single clockwise rotor (PS1) was present before the DC shock; shock appli-

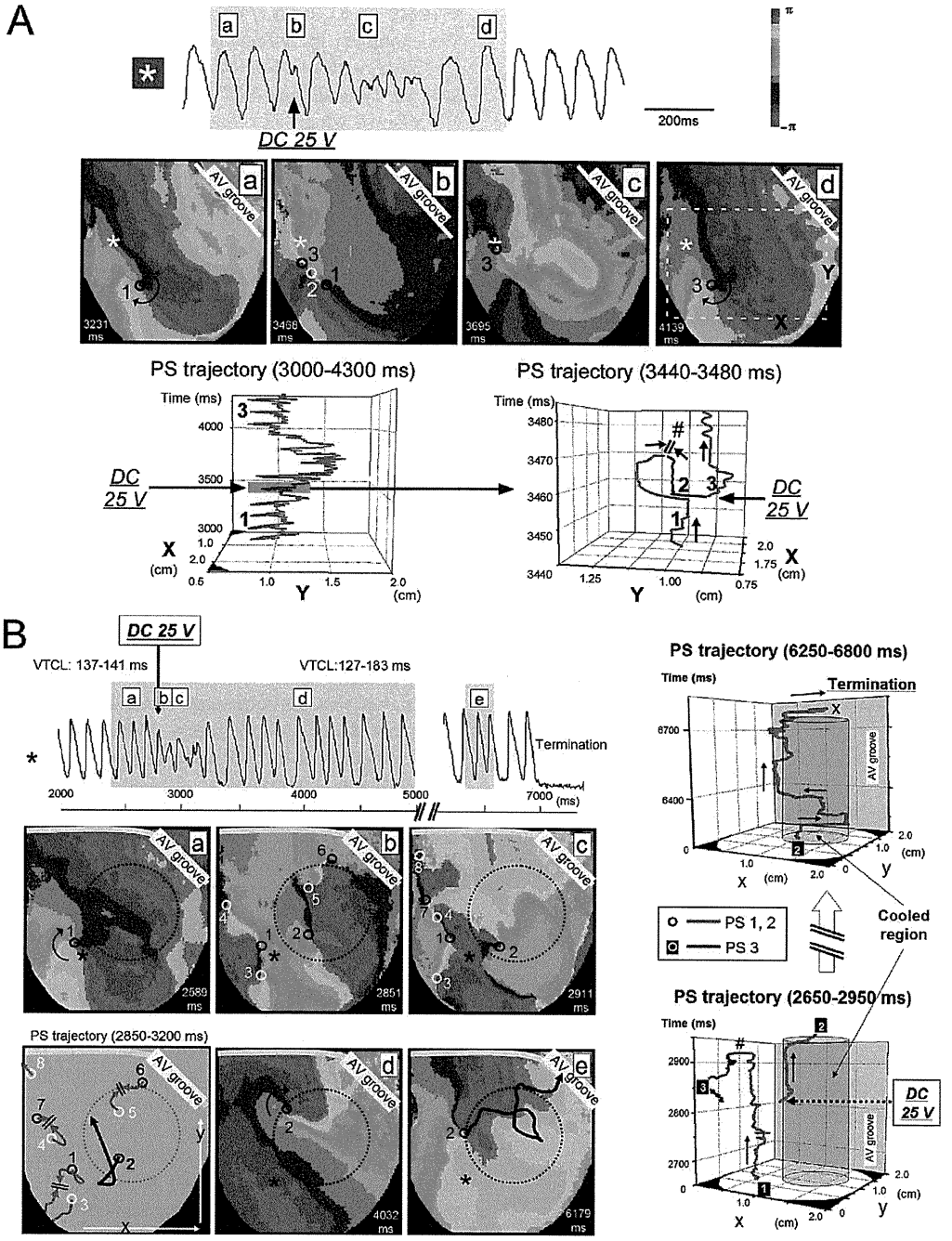

Figure 3 Rotor modification by DC shock applied to sustained VT in the absence and presence of RC. **A:** Failure of cardioversion by low-intensity shock in the absence of RC through repining of PS. Top, action potential trace; middle, phase maps before and after 25-V DC shock application. Black and white circles, PSs of clockwise and counterclockwise rotation, respectively. *Site of action potential recording. Bottom, trajectory of PSs plotted on space-time axes. A part of the trajectory in the left panel (immediately before and after DC shock application) is expanded in the right panel to show generation, mutual annihilation (#), and repining of PSs. **B:** Success of cardioversion by low-intensity DC shock in the presence of RC through unpinning of PS. Left, action potential trace (top) and phase maps (bottom) before (a) and after application of a 25-V DC shock (b–e). The shock application generated new PSs (black and white circles, clockwise and counterclockwise rotation, respectively). Trajectory of the PSs is illustrated in the right bottom panel. PS8 was pushed out of the observation area after meandering. PS1-PS3, PS4-PS7, and PS5-PS6 dissipated by mutual annihilation within 100 ms. PS2 survived and drifted in the periphery of the RC region (unpinning), and collided with the atrioventricular groove. *Site of action potential recording. Right, trajectory of PSs 1-3 plotted on space-time axes. Blue columns indicate the RC region. Abbreviations as in Figure 2.

cation generated a pair of PSs (counterclockwise PS2 and clockwise PS3). Then, PS1 and PS2 collided with each other and disappeared, whereas PS3 survived by anchoring and subsequently maintained the reentrant activity. Thus, as confirmed by the 3-D PS trajectory plots, the rotor dynamics were destabilized transiently by the DC shock, but restabilized after PS repining. In this heart, application of a 30-V DC shock resulted in generation of multiple PSs exhibiting irregular meandering, and the activation pattern was transformed from VT to VF (Online Supplementary Figure 3A), and application of a high-voltage (50 V) DC shock resulted in a prompt disappearance of reentrant activities by shock-induced phase resetting (Online Supplementary Figure 3B).

Figure 3B is the consequence of a 25-V DC shock, which terminated the reentrant activity in the presence of RC. Before the shock, a single clockwise rotor (PS1) anchored to a site close to the RC region (left, a). DC shock at 25 V created 7 new PSs (PSs2 to 8) of either chirality that meandered following complex trajectories (b and c). Then, PS1-PS3, PS4-PS7, and PS5-PS6 disappeared by mutual annihilation. PS8 moved out of the left margin (toward the posterior surface). PS2 survived and drifted along the periphery of the RC region (d and e). The VT terminated by collision of PS2 with the atrioventricular groove approximately 4 seconds after the DC shock application (top). Figure 3B, right, illustrates the trajectory of PSs plotted on space-time axes.

Figure 4 summarizes the data obtained from 18 sustained VTs (in 12 hearts) without RC and 13 sustained VTs (in 9 hearts) with RC exhibiting visible rotors; 38 and 17 DC shocks were applied without and with RC, respectively. In the cases of cardioversion failure, the mode of SW modification was classified into 3 types: no substantial change, repining of rotors (see Figure 3A), and transformation from VT to VF (see Online Supplementary Figure 3A). In the case of cardioversion success, the mode of SW modification was classified into 2 forms; unpinning of rotors followed by collision and extinction (see Figure 3B), and immediate disappearance of rotors by phase resetting (see Online Supplementary Figure 3B). As shown in Figure 4A, for DC shocks without RC (control), the major mode of success was phase resetting at high DC shock intensities ($\geq$50 V); transformation from VT to VF often occurred at intermediate intensities (30 to 40 V), and repining was the major mode of failure at relatively low intensities (20 to 30 V). For DC shocks with RC, in contrast, the major mode of success was unpinning with relatively low intensities (15 to 25 V), and the major mode of failure was no change. Figure 4B compares the success rate of DC cardioversion with and without RC. The intensity-response curve with RC was shifted to the left from that without RC (control) by 17.7 V. Average time to VT termination tended to be longer in the presence of RC (1.6 $\pm$ 1.9 seconds, n = 13) compared with that in the absence of RC (0.6 $\pm$ 1.2 seconds, n = 18), although the difference remained statistically insignificant (Figure 4C).

Effects of RC on VT/VF induced in 3-D hearts

We examined the effects of RC on the sustained VT/VFs (>120 seconds) in 6 intact hearts without cryoablation. A total of 17 sustained VT/VFs were induced. In 8 control VT/VFs, in which RC was not imposed, all (8 of 8) continued during the 30-second observation period. Subsequent application of biphasic DC shocks terminated 3 of 8 VT/VFs. In 9 VT/VFs, in which RC cardioversion was attempted, 1 of 9 terminated within 30 seconds by RC alone; subsequent application of DC shocks in the presence of RC terminated 7 of 8 VT/VFs. The threshold amplitude for the DC cardioversion was 56.7 $\pm$ 5.8 V (n = 3) in the absence of RC (control), and 31.4 $\pm$ 8.5 V (n = 7) in the presence of RC (P <.05). Time for cardioversion after DC application was 1.3 $\pm$ 1.7 seconds (n = 3) in the absence of RC and 12.2 $\pm$ 11.2 seconds (n = 7) in the presence of RC (P <.05). DC shocks at the maximum voltage (100 V) failed to terminate 5 of 8 VT/VFs in the absence of RC, but 1 of 8 in the presence of RC. Thus, RC facilitated cardioversion in 3-D hearts when combined with DC shocks in association with a certain modification of the mode of reentry termination.

Discussion

The major findings in the present study are as follows. First, rotors induced during RC were initially confined to the RC region, but were unstable and terminated early by collision following drift. Second, rotors underlying sustained VTs were transformed by RC from stationary to nonstationary; RC terminated approximately 50% of sustained VTs. Third, the threshold intensity of DC shocks for cardioversion of sustained VTs was reduced in the presence of RC; the major mode of rotor termination by DC shocks was changed from phase resetting to unpinning.

RC destabilizes rotors in favor of their termination

In the experiments in which VTs were induced during RC (the first protocol), 98% of the VTs self-terminated within 5 seconds because the rotors were unstable and drifted around the RC region. This finding, which is essentially concordant with a previous report by Boersma et al,[18] can be explained by creation of a region of long refractoriness and reduced conductivity by RC. During constant stimulation, RC prolonged the APD and decreased the CV in the RC region, which explained why the reentrant activity was impaired in the RC region, and was accompanied by intermittent conduction block and long tortuous PS meandering trajectories in the periphery of the RC region. We have previously demonstrated that global myocardial cooling (30°C to 33°C) caused an increase of the maximum APD restitution slope and a broadening of CV restitution curves compared with control subjects.[17] These changes of the restitution properties would increase destabilization of the reentry in the RC region through an enhancement of wavefront-tail interactions.[17] Temperature-dependent alterations of electrotonic effects, short-term memory, and perhaps intracellular Ca^{2+}

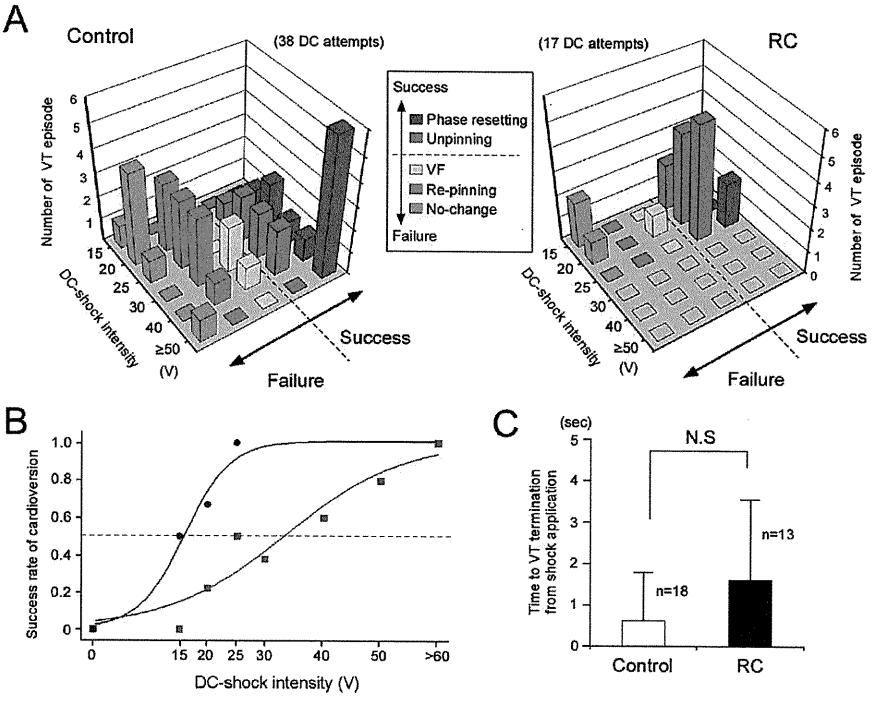

Figure 4 Modification of rotor dynamics by DC shocks applied to sustained VT. **A:** Intensity-dependent modification of rotor dynamics by DC shocks in the absence (control) and presence of RC. In the case of cardioversion success, the rotor modification was either phase resetting (red) or unpinning of PSs followed by collision and extinction (orange). When the cardioversion was failed, the rotor modification was either no substantial change (blue), repining of PSs (green) or transformation from VT to VF (yellow). **B:** Intensity-response of the success rate of DC cardioversion without (control, red) and with RC (blue). The shock intensity for 50% success was 33.3 V without RC (38 VTs) and 15.5 V with RC (18 VTs). **C:** Time required for VT termination from the instant of shock application without RC (control, n = 18) and with RC (n = 13, not significant). Abbreviations as in Figure 2.

dynamics might also contribute to rotor destabilization,[9] but such factors remain to be elucidated.

Mathematical model analysis of the rotor dynamics has demonstrated that spatial gradients in refractoriness play important roles in the stability of the rotation center in the cardiac muscle with normal excitability.[21–23] In a medium with stepwise heterogeneity, rotors move along the border separating regions with different refractoriness.[21] Our observation showing enormous PS drift in the periphery of the RC region is consistent with theoretical prediction.

To assess the potential usefulness of RC for cardioversion, we investigated the effects of RC on sustained VTs and found that RC terminated approximately 50% of sustained VTs. In the cases of successful cardioversion, the rotor dynamics changed dramatically from stationary to nonstationary. The nonstationary rotors shared common features with those induced after RC application in terms of long tortuous FBLs confined to the RC region and tremendous drift of rotors leading to their collision and extinction. The effects of RC on VT perpetuation were reversible upon removal of RC, suggesting a potential advantage of RC as a therapeutic procedure. The failure of RC cardioversion was attributable partly to the topological relationship between the pre-existing rotor and the RC region; when the rotation center was outside the RC region, the success rate of cardioversion was low. The RC cardioversion also depends on the size of the cooling area. In our pilot experiments, we tested the effects of RC to reduce the temperature by approximately 6°C from the baseline (36°C) in a circular area of 3 different size (5, 8, and 10 mm in diameter). Sustained VTs were terminated efficiently (16 of 33 VTs, 48%) by RC alone only with the largest size tested.

RC reduces the DC shock intensity required for cardioversion

When RC failed to terminate sustained VTs, we attempted DC cardioversion in the presence of RC. Those VTs were likely to be maintained by stationary rotors with PSs anchored at structural discontinuities. Our experiments showed that application of relatively low-intensity DC shocks always created new multiple PSs, resulting from shock-induced virtual electrode polarization.[24] SW reentry can be induced by a combination of depolarization and hyperpolarization at a close proximity.[24,25]

In control subjects (without RC), relatively weak DC shocks caused displacement of preexisting PSs (unpinning) and generated new PSs. Eventually such new PSs disappeared, but organized stationary SW reentry was resumed when the survived PSs were anchored again. Another mode of cardioversion failure was transformation from VT to VF, which was the result of irregular meandering of multiple, widely dispersed PSs. The major mode of cardioversion success in control subjects was immediate PS disappearance by phase resetting at intensities larger than the upper limit of vulnerability.[26] In contrast, when DC shocks of weak intensities were applied in the presence of RC, unpinning of PSs was not followed by repining. Instead, PSs drifted along the periphery of the RC region, eventually colliding and disappearing. Thus, the major mode of cardioversion success in the presence of RC was unpinning. The threshold shock

intensity was reduced significantly (by approximately 50%) from control subjects. Transformation from VT to VF rarely occurred in the presence of RC. These results suggest that RC facilitates DC cardioversion by confining and destabilizing rotors in the RC region.

Ripplinger et al[16] demonstrated in isolated rabbit right ventricular preparations that unpinning and destabilization of rotors leading to VT termination can be induced by weak DC shocks, provided that shocks are applied at a certain phase of the VT cycle.[16,22] A greater reduction of the DC shock intensity might be possible for cardioversion in combination with RC if the shocks were applied at a restricted phase. Further experimental studies are required to address the issue.

Study limitations

We showed facilitation of VT termination by RC in 2-D ventricular myocardium of rabbit hearts through unpinning and collision of rotors. We used BDM, which is known to affect ion channels and intracellular Ca^{2+} dynamics and to reduce muscle contraction. However, this does not seem to invalidate our results, because characteristic modification of rotor dynamics by RC was preserved in the absence of BDM (Online Supplementary Figure 5). Extrapolation of our observations in 2-D tissue preparations to 3-D and larger hearts is not straightforward. The chance of collision of rotors with boundaries would be reduced, and wave breakup would be enhanced in a larger 3-D tissue mass. In our experiments using intact 3-D rabbit hearts, in fact, RC alone was not effective for self-termination of sustained VT/VFs. However, the threshold intensity of DC shocks for cardioversion was significantly reduced in the presence of RC, and this was associated with an increase in the time required for cardioversion after the shock, suggesting alterations in the mode of reentry termination. Accordingly, a certain benefit of RC favoring low-energy defibrillation is considered to be preserved in 3-D hearts. Structural discontinuities and functional heterogeneities would alter the requirements for rotor termination. In addition, focal activities may also play roles in VT/VF.[27] To the best of our knowledge, there are no efficient RC devices applicable to clinical practice, and this is a critical issue to be solved in the future. Despite these limitations, the present study provides a new perspective toward the development of low-energy cardioversion/defibrillation.

Appendix

Supplementary data

Supplementary data associated with this article can be found, in the online version, at doi:10.1016/j.hrthm.2011.08.013.

References

1. Buxton AE, Lee KL, Fisher JD, Josephson ME, Prystowsky EN, Hafley G. A randomized study of the prevention of sudden death in patients with coronary artery disease. Multicenter Unsustained Tachycardia Trial Investigators. N Engl J Med 1999;341:1882–1890.
2. Lee DS, Green LD, Liu PP, et al. Effectiveness of implantable defibrillators for preventing arrhythmic events and death: a meta-analysis. J Am Coll Cardiol 2003;41:1573–1582.
3. Weaver WD, Cobb LA, Copass MK, Hallstrom AP. Ventricular defibrillation: a comparative trial using 175-J and 320-J shocks. N Engl J Med 1982;307:1101–1106.
4. Waldecker B, Brugada P, Zehender M, Stevenson W, Wellens HJ. Dysrhythmias after direct-current cardioversion. Am J Cardiol 1986;57:120–123.
5. Runsiö M, Kallner A, Källner G, Rosenqvist M. Bergfeldt L. Myocardial injury after electrical therapy for cardiac arrhythmias assessed by troponin-T release. Am J Cardiol 1997;79:1241–1245.
6. Godemann F, Butter C, Lampe F, et al. Panic disorders and agoraphobia: side effects of treatment with an implantable cardioverter/defibrillator. Clin Cardiol 2004;27:321–326.
7. Kamphuis HC, Verhoeven NW, Leeuw R, Derksen R, Hauer RN, Winnubst JA. ICD: a qualitative study of patient experience the first year after implantation. J Clin Nurs 2004;13:1008–1016.
8. Jalife J. Ventricular fibrillation: mechanisms of initiation and maintenance. Annu Rev Physiol 2000;62:25–50.
9. Weiss JN, Qu Z, Chen PS, et al. The dynamics of cardiac fibrillation. Circulation 2005;112:1232–1240.
10. Biktashev VN, Holden AV. Design principles of a low voltage cardiac defibrillator based on the effect of feedback resonant drift. J Theor Biol 1994;169:101–112.
11. Morgan SW, Plank G, Biktasheva IV, Biktashev VN. Low energy defibrillation in human cardiac tissue: a simulation study. Biophys J 2009;96:1364–1373.
12. Garfinkel A, Spano ML, Ditto WL, Weiss JN. Controlling cardiac chaos. Science 1992;257:1230–1235.
13. Pak HN, Liu YB, Hayashi H, et al. Synchronization of ventricular fibrillation with real-time feedback pacing: implication to low-energy defibrillation. Am J Physiol Heart Circ Physiol 2003;285:H2704–H2711.
14. Pak HN, Okuyama Y, Oh YS, et al. Improvement of defibrillation efficacy with preshock synchronized pacing. J Cardiovasc Electrophysiol 2004;15:581–587.
15. Ripplinger CM, Krinsky VI, Nikolski VP, Efimov IR. Mechanisms of unpinning and termination of ventricular tachycardia. Am J Physiol Heart Circ Physiol 2006;291:H184–H192.
16. Li W, Ripplinger CM, Lou Q, Efimov IR. Multiple monophasic shocks improve electrotherapy of ventricular tachycardia in a rabbit model of chronic infarction. Heart Rhythm 2009;6:1020–1027.
17. Harada M, Honjo H, Yamazaki M, et al. Moderate hypothermia increases the chance of spiral wave collision in favor of self-termination of ventricular tachycardia/fibrillation. Am J Physiol Heart Circ Physiol 2008;294:H1896–H1905.
18. Boersma L, Zetelaki Z, Brugada J, Allessie M. Polymorphic reentrant ventricular tachycardia in the isolated rabbit heart studied by high-density mapping. Circulation 2002;105:3053–3061.
19. Yamazaki M, Honjo H, Nakagawa H, et al. Mechanisms of destabilization and early termination of spiral wave reentry in the ventricle by a class III antiarrhythmic agent, nifekalant. Am J Physiol Heart Circ Physiol 2007;292:H539–H548.
20. Ishiguro YS, Honjo H, Opthof T, et al. Early termination of spiral wave reentry by combined blockade of Na^+ and L-type Ca^{2+} currents in a perfused two-dimensional epicardial layer of rabbit ventricular myocardium. Heart Rhythm 2009;6:684–692.
21. Fast VG, Kléber AG. Role of wavefront curvature in propagation of cardiac impulse. Cardiovasc Res 1997;33:258–271.
22. Fast VG, Rohr S, Gillis AM, Kléber AG. Activation of cardiac tissue by extracellular electrical shocks: formation of 'secondary sources' at intercellular clefts in monolayers of cultured myocytes. Circ Res 1998;82:375–385.
23. Kléber AG, Rudy Y. Basic mechanisms of cardiac impulse propagation and associated arrhythmias. Physiol Rev 2004;84:431–488.
24. Efimov IR, Cheng Y, Van Wagoner DR, Mazgalev T, Tchou PJ. Virtual electrode-induced phase singularity: a basic mechanism of defibrillation failure. Circ Res 1998;82:918–925.
25. Trayanova NA, Gray RA, Bourn DW, Eason JC. Virtual electrode-induced positive and negative graded responses: new insights into fibrillation induction and defibrillation. J Cardiovasc Electrophysiol 2003;14:756–763.
26. Gray RA, Chattipakorn N. Termination of spiral waves during cardiac fibrillation via shock-induced phase resetting. Proc Natl Acad Sci USA 2005;102:4672–4677.
27. Tabereaux PB, Dosdall DJ, Ideker RE. Mechanisms of VF maintenance: wandering wavelets, mother rotors, or foci. Heart Rhythm 2009;6:405–415.

Successful Catheter Ablation of Bidirectional Ventricular Premature Contractions Triggering Ventricular Fibrillation in Catecholaminergic Polymorphic Ventricular Tachycardia With *RyR2* Mutation

Takashi Kaneshiro, MD; Yoshihisa Naruse, MD; Akihiko Nogami, MD; Hiroshi Tada, MD; Kentaro Yoshida, MD; Yukio Sekiguchi, MD; Nobuyuki Murakoshi, MD; Yoshiaki Kato, MD; Hitoshi Horigome, MD; Mihoko Kawamura, MD; Minoru Horie, MD; Kazutaka Aonuma, MD

The subject of this report is a 38-year-old woman who often experienced syncope since childhood. Syncope occurred >10 times a year and was associated with convulsion during exercise and emotionally exciting situations. The patient's 13-year-old daughter had also experienced frequent episodes of syncope and developed ventricular fibrillation (VF) during treadmill exercise testing that was successfully defibrillated with electric shock. Witnessing this situation, the patient also lost consciousness, with documented VF that was converted to sinus rhythm by cardiopulmonary resuscitation without electric defibrillation.

Both the patient and her daughter were admitted to our hospital. We performed echocardiography, coronary angiography, and cardiac CT, the results of which revealed no structural heart disease. Resting 12-lead ECG did not indicate any abnormalities, including long-QT syndrome or Brugada syndrome. A signal-averaged ECG revealed no late potentials. Treadmill exercise testing easily induced bigeminal ventricular premature contractions (VPCs) with a right bundle branch block configuration and inferior axis (Figure 1A), and the exercise was terminated because of intolerable symptoms. Catecholamine stress test was started with administration of continuous intravenous infusion of epinephrine in a stepwise manner from 0.025 μg/kg per minute.[1] During epinephrine infusion at a rate of 0.1 μg/kg per minute, multifocal VPCs (VPC #1, right bundle branch block configuration and superior axis; VPC #2, right bundle branch block configuration and inferior axis [the same VPC configuration as that induced during the treadmill exercise testing]; and VPC #3, left bundle branch block configuration and inferior axis) appeared, and VPC #1 following VPC #2 subsequently induced VF (Figure 1B).

Administration of bisoprolol 5 mg QD was given but failed to suppress the exercise-induced bigeminal VPCs with the same morphology as induced previously. Because frequent deliveries of shock were believed to be likely, even with β-blocker treatment, catheter ablation was offered to the patient before implantable cardioverter-defibrillator (ICD) implantation. Catheter mapping and ablation for the bidirectional VPCs were performed with a 3D electroanatomic mapping system (CARTO; Biosense Webster) and a 3.5-mm-tip irrigation catheter (NaviStar; Thermo Cool) with only local anesthesia. No VPCs, ventricular tachycardia (VT), or VF were inducible with burst pacing and programmed stimulation from both right ventricular apex and right outflow tract during baseline and continuous intravenous infusion of isoproterenol.

With epinephrine infusion at a rate of 0.1 μg/kg per minute, VPC #1 and VPC #2 appeared. VPC #1 was nonsustained, and a presystolic Purkinje potential was recorded at the left ventricular inferoseptal area near the posteromedial papillary muscle, which preceded the onset of VPC #1 by 18 ms. The unipolar electrogram from the ablation catheter during VPC #1 showed a QS pattern, and a perfect match of the QRS configuration was obtained by pace mapping (Figure 2). Radiofrequency energy application to this site provoked some ventricular acceleration beats, and several radiofrequency energy applications around the target site finally eliminated all the VPCs, resulting in complete suppression of all VPC #1.

After the ablation of VPC #1, isolated occurrences of VPC #2 continued, and a local bipolar electrogram recorded on the left coronary cusp showed discrete prepotential that preceded the onset of VPC #2 by 65 ms, and a perfect match of the

Received July 26, 2011; accepted January 5, 2012.

From the Cardiovascular Division, Institute of Clinical Medicine (T.K., Y.N., H.T., K.Y., Y.S., N.M., K.A.) and Department of Child Health (Y.K., H.H.), Graduate School of Comprehensive Human Sciences, University of Tsukuba, Tsukuba, Japan; Division of Heart Rhythm Management, Yokohama Rosai Hospital, Yokohama, Japan (A.N.); and Department of Cardiovascular and Respiratory Medicine, Shiga University of Medical Science, Shiga, Japan (M.K., M.H.).

Correspondence to Kazutaka Aonuma, MD, Cardiovascular Division, Institute of Clinical Medicine, Graduate School of Comprehensive Human Sciences, University of Tsukuba, 1-1-1 Tennodai, Tsukuba, Ibaraki 305-8575, Japan. E-mail kaonuma@md.tsukuba.ac.jp

(*Circ Arrhythm Electrophysiol.* **2012;5:e14-e17.**)

Circ Arrhythm Electrophysiol **is available at http://circep.ahajournals.org** **DOI: 10.1161/CIRCEP.111.966549**

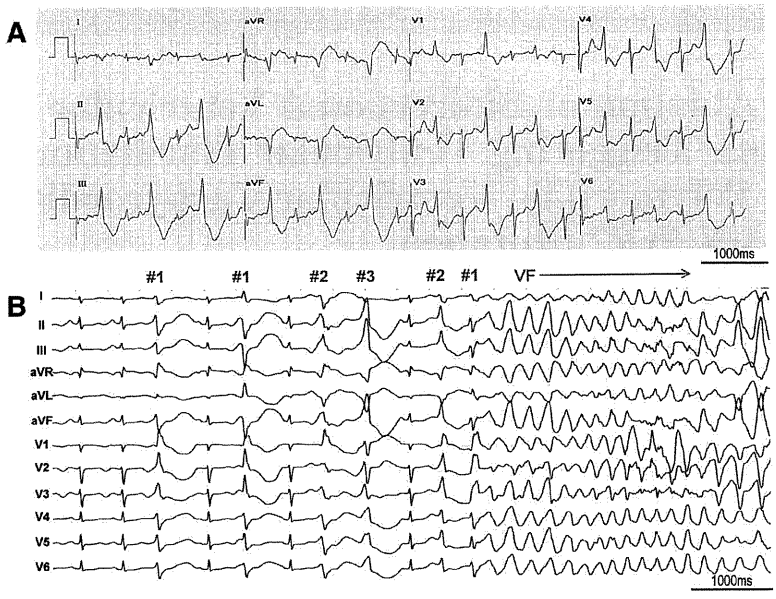

Figure 1. A, Twelve-lead ECG recording during treadmill exercise testing. Bigeminal ventricular premature contractions (VPCs) appeared during the second stage of the Bruce protocol. VPC morphology represented a right bundle branch block configuration and inferior axis. Because the patient experienced intolerable symptoms, the test was discontinued. **B**, Epinephrine stress test. Continuous intravenous infusion of epinephrine was started from a rate of 0.025 μg/kg per minute, and the QT interval did not changed. At a rate of 0.1 μg/kg per minute, VPC #1 (right bundle branch block configuration and superior axis), VPC #2 (right bundle branch block configuration and inferior axis, same as that induced in the treadmill exercise testing), and VPC #3 (left bundle branch block configuration and inferior axis) were induced. Subsequently, VPC #1 following VPC #2 suddenly induced ventricular fibrillation, which was successfully terminated with electric shock.

QRS configuration was obtained by pace mapping (Figure 3). Radiofrequency energy application to the left coronary cusp abolished VPC #2 4 s after the onset of radiofrequency energy application. After successful catheter ablation of bidirectional VPCs, neither VPCs nor VF were inducible, even with an infusion of epinephrine of up to 1.2 μg/kg per minute (a >10 times higher dose than provocation). Precise ablation sites in a 3D electroanatomic mapping merged with contrast-enhanced CT are shown in Figure 4.

ICD implantation was performed, and the patient was discharged from the hospital on bisoprolol 2.5 mg QD. Serial Holter ECGs after the ablation showed only 3 to 5 isolated VPCs with a different morphology from the previously observed VPCs, and treadmill exercise testing induced no VPCs at the maximal workload. During 16-month follow-up, neither episodes of syncope nor ICD therapy occurred. Genetic analysis revealed a mutation in the ryanodine receptor gene (*RyR2*), and a diagnosis of catecholaminergic polymorphic VT (CPVT) was confirmed (Figure 5).[2] The patient's daughter was also given a diagnosis of CPVT with same mutation in *RyR2* and had catheter ablation for the origins of bidirectional VT. Although she refused ICD

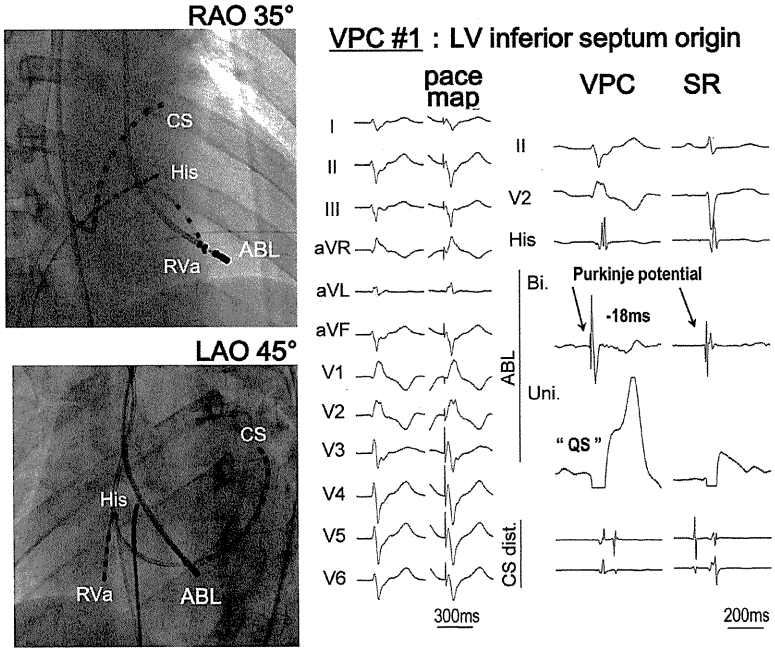

Figure 2. Activation mapping and pace mapping for VPC #1. A Purkinje potential was recorded from the left ventricular inferoseptum and preceded the QRS onset by 18 ms. The unipolar electrogram recorded from the distal electrode showed a QS pattern. Perfect pace mapping was obtained at this site. ABL indicates ablation catheter; CS, coronary sinus; His, His bundle; LAO, left anterior oblique; RAO, right anterior oblique; RVa, right ventricular apex; SR, sinus rhythm; VPC, ventricular premature contraction.

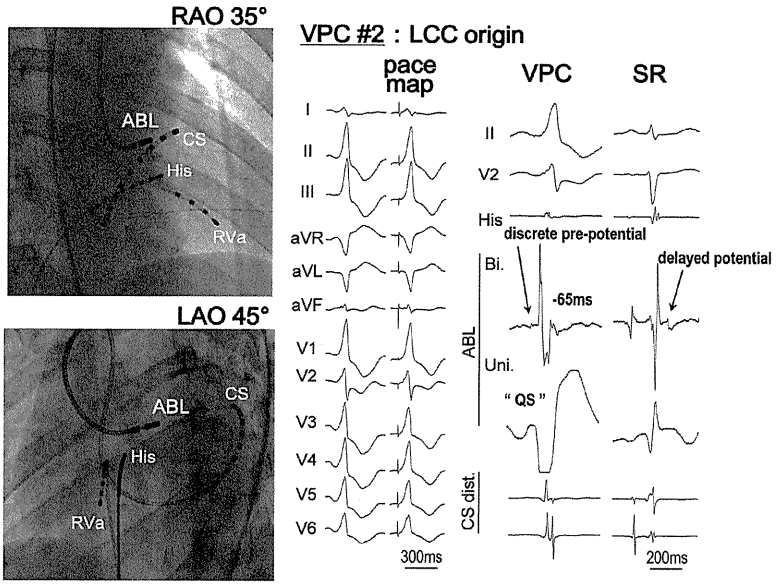

Figure 3. Activation mapping and pace mapping for VPC #2. A local bipolar electrogram recorded from the LCC showed a discrete prepotential that preceded the QRS onset by 65 ms associated with a QS pattern of unipolar electrogram. Perfect pace mapping was obtained at this site. ABL indicates ablation catheter; CS, coronary sinus; His, His bundle; LAO, left anterior oblique; LCC, left coronary cusp; RAO, right anterior oblique; RVa, right ventricular apex; SR, sinus rhythm; VPC, ventricular premature contraction.

implantation, she had not experienced any episode of VT or syncope with β-blocker treatment.

The generally accepted therapy for CPVT has been β-blockers,[3] and the additional administration of flecainide or verapamil to β-blockers has been reported to be effective; however, the effects of those drugs are not fully standardized. For medically refractory cases, sympathetic denervation is one of the alternative treatment options. The ICD is considered the definitive therapy for the prevention of sudden cardiac death; however, failure to prevent sudden cardiac death has been reported in several cases because ICD shock delivery might lead to catecholamine release, resulting in an electric storm.[4] This concern prompted the decision to attempt catheter ablation of VPCs triggering VF. Although several reports have described successful catheter ablation of VPCs triggering VF in some patients with structurally normal hearts, such as those with Brugada syndrome, long-QT syndrome, and idiopathic VF, successful catheter ablation of VPCs triggering VF in CPVT has not been reported. Cerrone and colleagues[5] reported that the mechanism of CPVT was due to the delayed afterdepolarization-induced triggered activity in a focal Purkinje network in a knock-in (*RyR2*) mouse. However, whether the Purkinje system is related to the mechanism of VF in CPVT or just trigger origin is still unknown.

To our knowledge, this is the first report of successful catheter ablation of the bidirectional VPCs that trigger VF, and this procedure could become one of the adjunctive

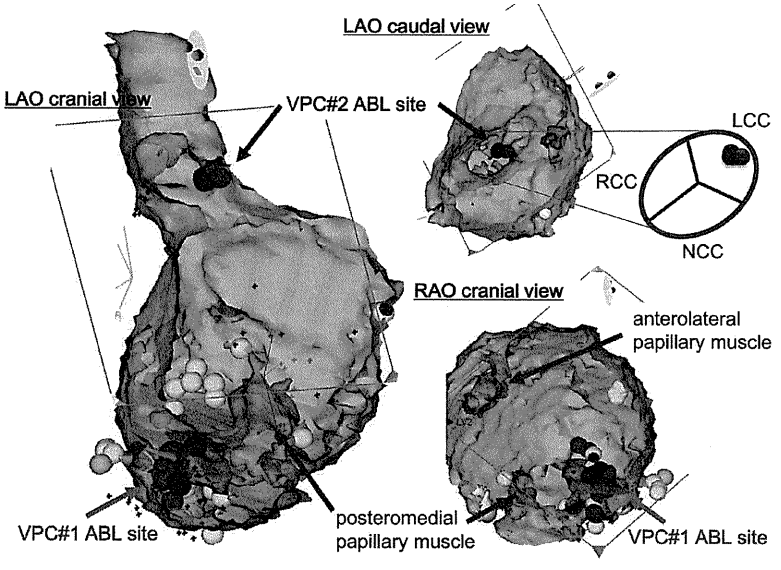

Figure 4. Electroanatomic mapping merged with contrast-enhanced CT. Red tags indicate the ABL sites. Blue tags indicate the sites with perfect pace mapping, and yellow tags indicate the sites with Purkinje potentials during sinus rhythm. The sites with perfect pace mapping and the earliest activation for VPC #1 were localized in the inferoseptal site adjacent to the base of the posteromedial papillary muscle (red arrow). Successful ablation site of VPC #2 was on the left coronary cusp (blue arrow). ABL indicates ablation; LAO, left anterior oblique; LCC, left coronary cusp; NCC, noncoronary cusp; RAO, right anterior oblique; RCC, right coronary cusp; VPC, ventricular premature contraction.

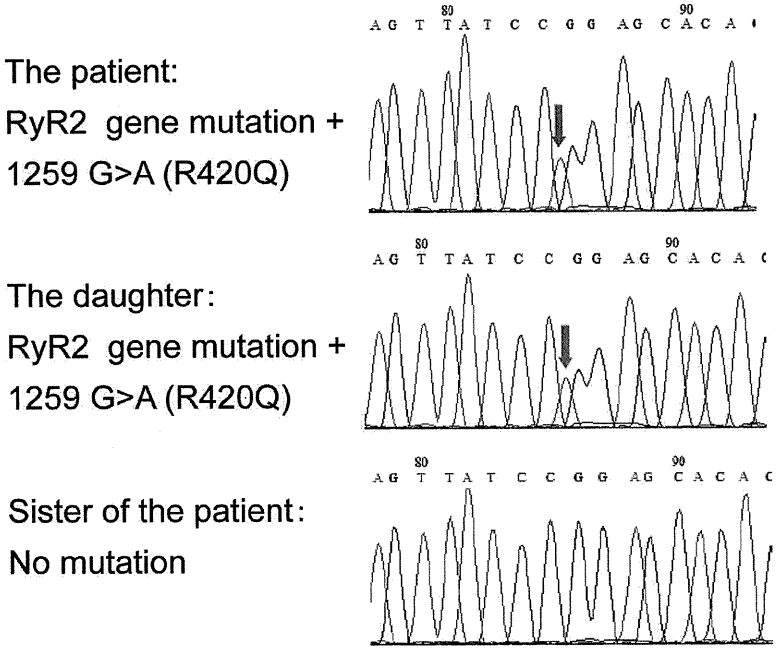

Figure 5. Results of genetic analysis. A mutation in the ryanodine receptor gene (*RyR2*) was detected in both the patient and her daughter. The mutation was not detected in the patient's sister.

therapies in patients with CPVT. To clarify the effectiveness and safety of this procedure, more cases and longer-term observation are mandatory.

Disclosures

None.

References

1. Krahn AD, Gollob M, Yee R, Gula LJ, Skanes AC, Walker BD, Klein GJ. Diagnosis of unexplained cardiac arrest: role of adrenaline and procainamide infusion. *Circulation.* 2005;112:2228–2234.
2. Priori SG, Napolitano C, Tiso N, Memmi M, Vignati G, Bloise R, Sorrentino V, Danieli GA. Mutations in the cardiac ryanodine receptor gene (*hRyR2*) underlie catecholaminergic polymorphic ventricular tachycardia. *Circulation.* 2001;103:196–200.
3. Sumitomo N, Harada K, Nagashima M, Yasuda T, Nakamura Y, Aragaki Y, Saito A, Kurosaki K, Jouo K, Koujiro M, Konishi S, Matsuoka S, Oono T, Hayakawa S, Miura M, Ushinohama H, Shibata T, Niimura I. Catecholaminergic polymorphic ventricular tachycardia: electrocardiographic characteristics and optimal therapeutic strategies to prevent sudden death. *Heart.* 2003;89:66–70.
4. Mohamed U, Gollob MH, Gow RM, Krahn AD. Sudden cardiac death despite an implantable cardioverter-defibrillator in a young female with catecholaminergic ventricular tachycardia. *Heart Rhythm.* 2006;3:1486–1489.
5. Cerrone M, Noujaim SF, Tolkacheva EG, Talkachou A, O'Connell R, Berenfeld O, Anumonwo J, Pandit SV, Vikstrom K, Napolitano C, Priori SG, Jalife J. Arrhythmogenic mechanisms in a mouse model of catecholaminergic polymorphic ventricular tachycardia. *Circ Res.* 2007;101:1039–1048.

KEY WORDS: catecholaminergic polymorphic ventricular tachycardia ■ catheter ablation ■ arrhythmia

Clinical and electrocardiographic characteristics of patients with short QT interval in a large hospital-based population

Akashi Miyamoto, MD, PhD,* Hideki Hayashi, MD, PhD,* Tomohide Yoshino, MD,* Tamiro Kawaguchi, MD,* Atsushi Taniguchi, MD,* Hideki Itoh, MD, PhD,* Yoshihisa Sugimoto, MD, PhD,* Makoto Itoh, MD, PhD,* Takeru Makiyama, MD, PhD,† Joel Q. Xue, PhD,‡ Yoshitaka Murakami, PhD,§ Minoru Horie, MD, PhD*

*From the *Department of Cardiovascular and Respiratory Medicine, Shiga University of Medical Science, Otsu, Shiga, Japan, †Department of Cardiovascular Medicine, Kyoto University Graduate School of Medicine, Kyoto, Kyoto, Japan, ‡General Electric Healthcare, Milwaukee, Wisconsin, §Department of Health Science, Shiga University of Medical Science, Otsu, Shiga, Japan.*

BACKGROUND Short QT syndrome is one of the underlying disorders associated with ventricular fibrillation. However, the precise prognostic implication of a short QT interval remains unclear.

OBJECTIVE The purpose of this study was to investigate the prevalence and long-term prognosis in patients with a shorter-than-normal QT interval in a large hospital-based population.

METHODS We chose patients with a short Bazett QTc interval from a database consisting of 114,334 patients to determine the clinical characteristics and prognostic value of a short QT interval.

RESULTS A total of 427 patients (mean age 43.4 ± 22.4 years) had a short QT interval with about a 1.2 times higher male predominance (234 men). The QTc interval was significantly longer in female than in male patients (363.8 ± 6.1 ms vs 357.1 ± 5.8 ms, $P < .0001$). The age-specific prevalence of patients with short QT interval was biphasic, peaking at young and old age. Atrial fibrillation and early repolarization were complicated with short QT interval in 39 (9.1%) and 26 (6.1%) patients, respectively. The prognosis of 327 patients (182 men; mean age, 46.4 ± 27.3 years) with a short QT interval could be assessed (mean follow-up period, 54.0 ± 62.0 months). During the follow-up, 2 patients, 1 of whom had early repolarization, developed life-threatening events, in contrast to 6 patients who died of noncardiac causes and did not have early repolarization.

CONCLUSION The prevalence of a short QT interval showed a slight male preponderance and biphasic age-dependent distribution in both genders. The complication rate of atrial fibrillation was higher in those with a short QT interval than in general populations. The long-term outcome suggested that early repolarization in a short QT interval might be associated with potential risk of lethal arrhythmia.

KEYWORDS Electrocardiography; QT interval; Prevalence; Prognosis; Repolarization

ABBREVIATIONS **AF** = atrial fibrillation; **CI** = confidence interval; **ECG** = electrocardiogram

(Heart Rhythm 2012;9:66–74)

Introduction

The QT interval is an invaluable prognostic marker for evaluating whether ventricular arrhythmia occurs.[1–3] Long QT syndrome is characterized by ventricular cells that fail to repolarize sufficiently quickly. On the other hand, short QT syndrome manifests an extremely abbreviated QT interval.[4,5] Genetic mutations underlie both syndromes, in which sudden cardiac death occurs.[6,7] It was reported that short QT syndrome complicated other electrocardiogram (ECG) abnormalities, such as atrial fibrillation (AF)[4] and early repolarization.[8] Although close attention must be paid to short QT interval, there may be overlap between normal QT interval and abnormally short QT interval.[9] In addition, the prognostic value of short QT syndrome in relation to AF or early repolarization is yet to be determined.

In our university hospital, more than 350,000 ECGs obtained from more than 110,000 patients are available for digital analysis. Using this large hospital-based population, we aimed: (1) to determine the distribution of the QT interval in the entire population, (2) to determine the clinical and ECG characteristics in individuals with short QT interval, and (3) to investigate the prognostic value of short QT interval.

Methods

The research protocol was approved by the Ethical Committee of Shiga University of Medical Science.

Address reprint requests and correspondence: Dr. Hideki Hayashi, Department of Cardiovascular and Respiratory Medicine, Shiga University of Medical Science, Otsu, Shiga 520-2192, Japan. E-mail address: hayashih@belle.shiga-med.ac.jp.

1547-5271/$ -see front matter doi:10.1016/j.hrthm.2011.08.016

Database

We analyzed resting 12-lead ECGs recorded in the university hospital of Shiga University of Medical Science. The 114,334 consecutive patients (55,091 female and 59,243 male patients) who had undergone ECG recordings between January 1983 and July 2010 were enrolled in the present study. A total number of 359,737 ECG recordings were obtained during this period. The 12-lead ECG was recorded for 10 seconds at a sweep speed of 25 mm/s, calibrated to 1 mV/cm in the standard leads. Twelve leads were simultaneously acquired. The ECG signals were recorded with a temporal sampling interval of 2 ms (i.e., 500 Hz). Digital data were stored in a server computer with 12-bit resolution.

Digital analysis of ECG

MUSE7.1 (GE Marquette Medical Systems, Inc., Milwaukee, Wisconsin) detected an identical P wave and QRS complex with a template matching technique. When AF (defined as irregular RR intervals with fibrillatory waves) was present, only QRS complex was identified by template-matching technique. ECG variables measured were composed by the averaged value during a 10-second recording time. QT interval was measured from the earliest detection of depolarization in any lead (QRS onset) to the latest detection of repolarization in any lead (T wave offset). T wave offset was determined by the time when 98% of the integrated area of T wave was over, which corresponded to a point where the T wave downsloping limb nearly joined the baseline. U wave was excluded. The QTc interval was calculated after correction for heart rate with the Bazett formula. Early repolarization was defined as an elevation at the junction between QRS complex and ST-segment $\geq$0.1 mV from baseline level in at least 2 leads. ST-segment elevation should be present in at least 2 consecutive beats to identify early repolarization. ECG recordings of a mean heart rate <50 or >100 beats/min were excluded from the analysis in the first analysis, and then the prevalence of short QT interval in patients with sinus bradycardia <50 beats/min was additionally investigated. ECGs with ventricular pacing were also excluded. Because all measurements of 12-lead ECG were digitally performed by virtue of software, neither intraobserver nor interobserver variability occurred in this study. To determine whether the automatic measure of QT interval correlates with the manual measure of QT interval, 1,000 ECGs were randomly selected, and then we compared the automatic and manual measure of the QT interval. The manual measure of the QT interval was performed by a standard tangential method in lead V5. The manual QT interval measurement was obtained by averaging the QT interval of 3 consecutive beats.

Data analysis

First, we constructed histograms according to QTc interval. QTc interval divided by 5 ms and the number of ECGs or patients used for frequency density were shown on the abscissa and the ordinate, respectively. Second, the prevalence of patients with a short QTc interval in association with age and gender was determined. Third, clinical and ECG characteristics of patients with a short QTc interval were determined. The prevalence of AF and early repolarization complicated by short QT interval was determined. Fourth, the prognostic value of a short QTc interval was assessed. Long-term outcome was determined by assessing whether sudden cardiac death, life-threatening ventricular arrhythmia, or any cause of death occurred. Patients were considered to have died suddenly if death was observed and had occurred within 1 hour after new or more serious complaints of probable cardiovascular cause. Life-threatening ventricular arrhythmia was determined by documented ECG. We reviewed the medical records of patients with short QT interval to evaluate their physical health status. In patients whose medical records were not available to determine prognosis, we gathered information on health status by a postal questionnaire. We performed gene analysis (see Supplementary Materials) in patients who developed life-threatening events with short QT interval.

Statistical analysis

The data are presented as mean ± SD. A comparison between 2 groups was performed with the Student t test or the nonparametric Mann-Whitney U test, as appropriate. Categorical variables were compared with χ^2 test. Kolmogorov-Smirnov test was performed to determine whether QTc interval distribution fit to a normal distribution. All tests were 2-tailed, and a value of P <.05 was considered statistically significant.

Results

In the database, there were 11,416 and 21,450 ECGs with heart rate of <50 and >100 beats/min, respectively. We excluded these ECGs from this study, thus 301,345 ECGs derived from 105,824 patients (56.0% men; mean age, 52.6 ± 20.7 years) were included for the analysis of this study. The autonomic QT interval measure was a little but significantly longer than the manual QT interval measure (421.8 ± 23.2 ms vs 418.0 ± 24.5 ms, P <.0001).

The mean difference between the manual and automatic QT interval measure was 3.8 ms (median 3.7 ms), and there was a significant linear correlation (r = 0.95, P <.00001) between the manual and autonomic measure of QT interval (Supplementary Figure 1), indicating the accuracy of the computer-assessed measure of QT interval.

Prevalence of QT interval

Figure 1 shows the distribution of the QTc intervals of total, male, and female patients. The histograms that were constructed as a function of the number of ECGs are shown in the upper row of Figure 1. The mean QTc interval was 421.4 ± 25.7 ms (95% confidence interval [CI] 382 to 482 ms, range 329 to 693 ms) in total patients; 418.9 ± 25.7 ms (95% CI 380 to 480 ms, range 331 to 693 ms) in male patients; and 424.7 ± 25.3 ms (95% CI 387 to 483 ms, range 329 to 687 ms) in female patients. The QTc interval was significantly (P <.0001) longer in female patients than

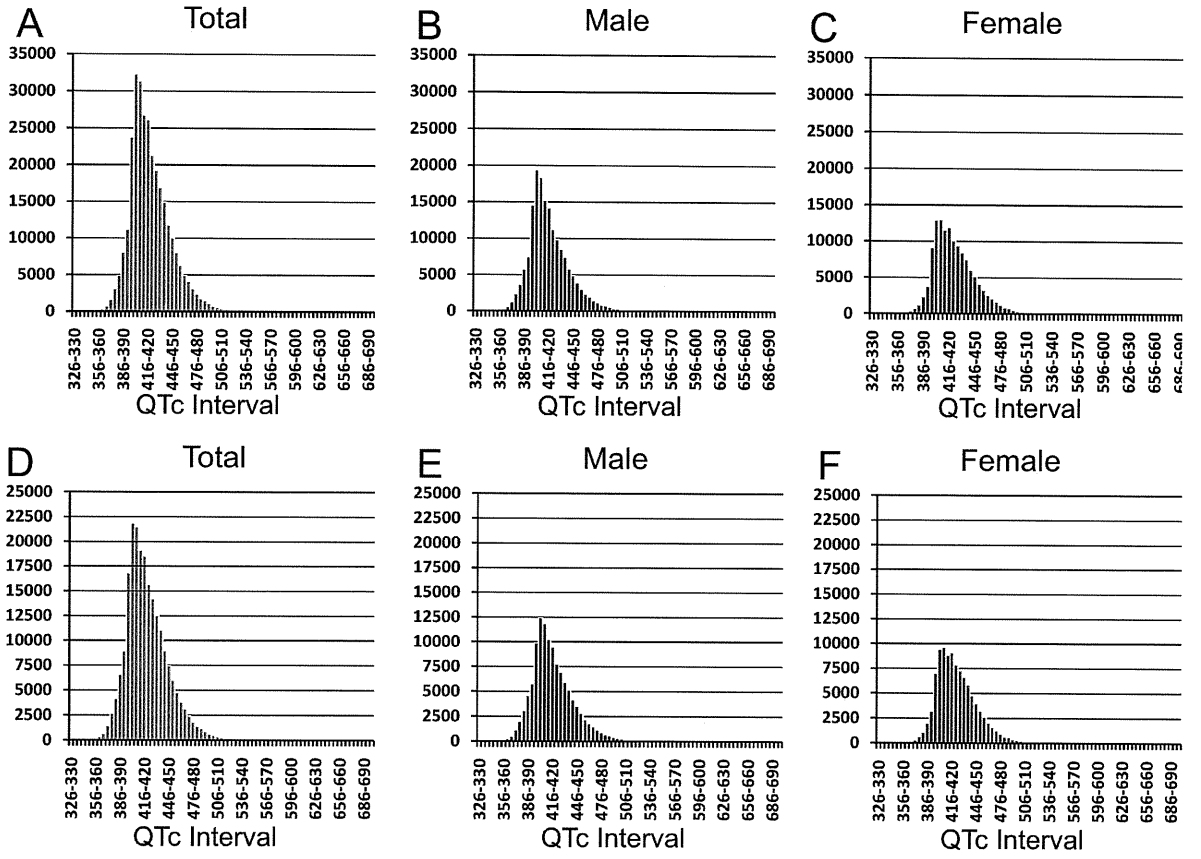

Figure 1 Distribution of Bazett QTc interval according to the number of patients (upper row) and the number of ECGs (lower row). Histograms of total, male, and female patients in this study population are displayed in panels A and D, B and E, and C and F, respectively.

in male patients. The QTc interval distributions did not fit a normal distribution curve ($P < .01$ for each) because the distributions were asymmetrical and right skewed. The histograms of QTc interval that were generated as a function of the number of patients are shown in the lower row of Figure 1. Similarly, the histograms of the QTc interval were right-skewed, which failed to fit to a normal distribution ($P < .01$ for each). The mode of QTc interval was 401 to 405 ms (range 329 to 693 ms), 401 to 405 ms (range 331 to 693 ms), and 406 to 410 ms (range 329 to 687 ms) in total, male, and female patients, respectively. Table 1 shows the lowest percentiles of QTc interval. The QTc interval at the lowest 2.5 percentile was longer than the lower limit of normal QTc interval previously reported.[9] The QTc interval[10,11] at the lowest 0.15 percentile was similar to the lower border of QTc interval. We therefore adopted a definition of short QT on the basis of previous studies, the cutoff value matching the 0.15 percentile of our whole population (234 male patients with QTc interval ≤362 ms, 193 female patients with QTc interval ≤369 ms). Furthermore, we divided the short QT population into percentiles and selected the 2.5 percentile of the short QT population as the very short QT (Table 2).

Clinical characteristics of short QT interval

Four hundred twenty-seven patients with short QT interval were chosen for the analysis according to the abovementioned rationale. The prevalence of patients with a short QT interval was about 1.2 times higher in male patients (N = 234) than in female patients (N = 193). The mean age was not different between male and female patients (41.9 ± 21.5 years vs 45.2 ± 23.4 years). Table 3 shows clinical characteristics of the patients with short and very short QTc intervals. The mean age was not different between short and

Table 1 The lowest percentiles of Bazett QTc interval for this study population

	Bazett QTc interval (ms)	
Percentile	Male	Female
2.5	380.0	387.0
2.0	378.0	386.0
1.0	373.0	381.0
0.5	369.0	376.0
0.15	362.0	369.0
0.1	361.0	367.0
0.0	331.0	329.0